AN ABSTRACT OF THE THESIS OF

Alex LaFranchi for the degree of Honors Baccalaureate of Science in Mechanical Engineering presented on May 26, 2015. Title: CFD Model Analysis and Validation for a Formula SAE Racecar.

Abstract approved:

_____

Robert K. Paasch

This project examines the computational fluid dynamics (CFD) model used by Global Formula Racing (GFR) to simulate external aerodynamics for a Formula SAE racecar. It seeks to improve the accuracy of the existing model by changing mesh and physics model parameters. Accuracy of the model is quantified through comparison to physical experimental data. Mesh parameters studied include prism layer properties, wake refinement, and volumetric control use. Multiple turbulence models are compared, and sensitivity to initial conditions and boundary conditions is quantified. A recommended half-car mesh and physics model is produced, and recommendations for further development are added.

Key Words: CFD, Aerodynamics, Formula SAE

Corresponding e-mail address: a.lafranchi@gmail.com

CFD Model Analysis and Validation for a Formula SAE Racecar

by
Alex LaFranchi

A PROJECT

submitted to

Oregon State University

University Honors College

in partial fulfillment of
the requirements for the
degree of

Honors Baccalaureate of Science in Mechanical Engineering
(Honors Scholar)

Presented May 26, 2015
Commencement June 2015

Honors Baccalaureate of Science in Mechanical Engineering project of Alex LaFranchi presented on May 26, 2015.

APPROVED:

Robert K. Paasch, Mentor, representing Mechanical Engineering

Nancy Squires, Committee Member, representing Mechanical Engineering

Phillip Arscott, Committee Member, representing Mechanical Engineering

Toni Doolen, Dean, University Honors College

I understand that my project will become part of the permanent collection of Oregon State University, University Honors College. My signature below authorizes release of my project to any reader upon request.

Alex LaFranchi, Author

Acknowledgements

I would like to thank Dr. Paasch for his consistent support of my thesis project and GFR. He is a very enthusiastic and helpful mentor, and has created an excellent learning environment for me and many other engineering students. I would also like to thank Phil Arscott for his help and advice working closely with me on my thesis and many other GFR projects. I also extend my thanks to Dr. Squires for her help on my thesis committee, and for her outstanding commitment to teaching and mentoring any student who comes to her door.

Contents

1. Project Description

1.1 Introduction

Global Formula Racing (GFR) is a student team that is a cooperative between Oregon State University (OSU) and Duale Hochschule Baden Württemberg Ravensburg (DHBW-R). GFR competes in Formula SAE, a student competition which challenges students to design, manufacture, and race formula-style cars in a variety of events. Each year, GFR designs and manufactures two new cars which improve on the previous year's design and comply with the most recent Formula SAE rules. The two cars share many of the same features, such as chassis, suspension, and some or all aerodynamic elements. The cars differ in that one has a combustion powertrain (cCar) and the other has an electric powertrain (eCar). OSU focuses more on the cCar and DHBW-R focuses more on the eCar, but both schools are very involved in the design and manufacture of both cars.

GFR competes in Formula SAE at locations in the US and Europe. Traditionally, GFR competes in Michigan, Germany, and Austria every year, and has also competed in Spain, Italy, the UK, and California. These competitions are divided into eight events. Teams receive scores for each event, and the team with the most total points wins the competition. There are three static events (engineering design, cost analysis, and business presentation) worth a total of 325 points and five dynamic events (acceleration, skidpad, autocross, efficiency, and endurance) worth a total of 675 points. The static events challenge students to make good engineering decisions, a cost effective car, and a hypothetical business plan to sell it. Students must present and defend these decisions and plans during these events at competition. The dynamic events test a car's on-track performance and qualities such as forward acceleration, lateral acceleration, braking, and reliability. This division of points means that the car that is the fastest or best in any particular event is not necessarily a good car for the whole competition. Students must critically assess the point structure and evaluate which qualities will make a car an overall winner and which qualities are less important.

GFR's goal is to win competitions. It has been very successful in this goal, with 13 wins in the last five years, including all of the competitions it entered in 2014. It approaches this goal by focusing on improving the car in the most point-sensitive areas. Point sensitivity is determined by a student-built lap simulation [1] which varies parameters such as mass, power, downforce, and drag and reports the estimated effect on points. GFR has a philosophy of simplicity, reliability, and simulation validated by physical testing. Point sensitivity studies and the GFR philosophy guide GFR's overall vehicle concept: a lightweight car with a single-cylinder engine and a lot of downforce.

Downforce has been shown to be the most point-sensitive parameter on the car. Because of this, it is very important for the wings to perform well. It is difficult to evaluate wing performance analytically. There are many complex interactions between aerodynamic elements, and the flow behavior is not always intuitive. Therefore, we rely on computer simulation and physical testing to objectively compare different aerodynamic concepts and create downforce and drag estimates.

Computational fluid dynamics (CFD) tools are used to simulate airflow around the car. GFR uses Star-CCM+, a CFD program published by CD-adapco.

This project will work to gain a better understanding of the different tools and models available in Star-CCM+. Since 2011, GFR has performed several dedicated studies to improve the efficiency and accuracy of our Star-CCM+ model. However, there are still many parameters that we do not fully understand. In this project, I will first research these parameters to gain an understanding of what they do, when they should be used, and which are appropriate for GFR. I will then complete sensitivity studies to refine the mesh settings and physics models and determine what effect these settings have on the simulation. These simulations will be performed on standard airfoils for which wind tunnel data is readily available, and the CFD results will be compared to published wind tunnel results. The simulations will also be performed on the full car model and the results will be compared to past years' simulations and physical testing results. This project will ultimately deliver a recommended CFD model to use in future years. This model should accurately represent the aerodynamic properties of the car and use a reasonably low amount of processing power. This will benefit the team by giving it more accurate results from CFD simulations, which will allow it to develop better aero packages and earn more points.

1.2 Rules and Constraint Analysis

Rules in bold are taken from the 2015 Formula SAE Rules [2]. The rules listed restrict the aerodynamics package in various ways.

T1.2.2
Once the vehicle is approved to compete in the dynamic events, the ONLY modifications permitted to the vehicle are those listed below. They are also referred to in Part S of the Formula SAE Rules–Static Event Regulations.

- **a. Adjustment of belts, chains and clutches**
- **b. Adjustment of brake bias**
- **c. Adjustment of the driver restraint system, head restraint, seat and pedal assembly**
- **d. Substitution of the head restraint or seat insert for different drivers**
- **e. Adjustment to engine operating parameters, e.g. fuel mixture and ignition timing, and any software calibration changes**
- **f. Adjustment of mirrors**
- **g. Adjustment of the suspension where no part substitution is required, (except that springs, sway bars and shims may be changed)**
- **h. Adjustment of tire pressure**
- **i. Adjustment of wing angle, but not the location**
- **j. Replenishment of fluids**
- **k. Replacement of worn tires or brake pads. Replacement tires and brake pads must be identical in material/composition/size to those presented and approved at Technical Inspection.**

l. **The changing of wheels and tires for "wet" or "damp" conditions as allowed in Part D of the FSAE Rules–Dynamic Event Regulations.**
m. **Recharging low voltage batteries**
n. **Recharging high voltage accumulators**

Per T1.2.2.i, the wing location cannot be changed during competition, but wing angles can. This means that to be able to optimize downforce and drag for different events, we need to design wings that are sensitive to changes in angle of attack. For example, we want wings that can be adjusted to a low drag setting for the acceleration event and a high downforce setting for skidpad.

T2.1
Vehicle Configuration
The vehicle must be open-wheeled and open-cockpit (a formula style body) with four (4) wheels that are not in a straight line.

Definition of "Open Wheel"–Open Wheel vehicles must satisfy all of the following criteria:

a. **The top 180 degrees of the wheels/tires must be unobstructed when viewed from vertically above the wheel.**
b. **The wheels/tires must be unobstructed when viewed from the side.**
c. **No part of the vehicle may enter a keep-out-zone defined by two lines extending vertically from positions 75mm in front of and 75mm behind, the outer diameter of the front and rear tires in the side view elevation of the vehicle, with tires steered straight ahead. This keep-out zone will extend laterally from the outside plane of the wheel/tire to the inboard plane of the wheel/tire. See the figure** [Figure 1.1] **"Keep out Zones" below.**
d. **Must also comply with the dimensions/requirements of Article 9 Aerodynamic devices.**

NOTE: The dry tires will be used for all inspections.

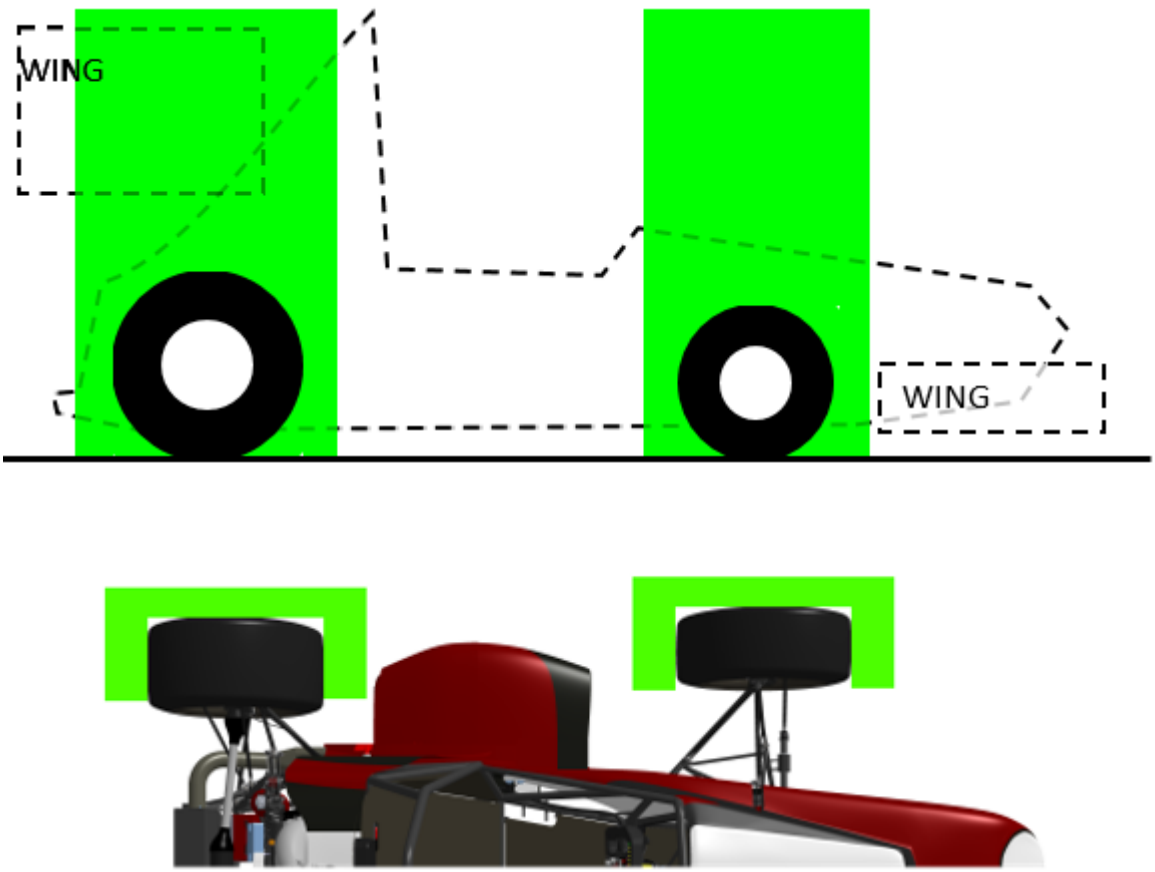

Figure 1.1: “Keep out zones”

Rule T2.1 restricts the location of aerodynamic devices relative to the wheels. It prevents us from placing any aerodynamic devices above the wheels at any height or in a “keep out zone” in front of and behind the wheels. These restricted areas are shown in green in Figure 1.1. This rule is more restrictive than last year and will require the aerodynamic package to be shrunk to fit in the new allowable area.

T4.8 Driver Egress

All drivers must be able to exit to the side of the vehicle in no more than 5 seconds. Egress time begins with the driver in the fully seated position, hands in driving position on the connected steering wheel and wearing the required driver equipment. Egress time will stop when the driver has both feet on the pavement.

Rule T4.8 requires that the driver be able to exit the vehicle quickly. This prevents us from using any side wings in places that would make quick egress difficult.

T6.2 Ground Clearance

Ground clearance must be sufficient to prevent any portion of the car, other than the tires, from touching the ground during track events. Intentional or excessive ground contact of any portion of the car other than the tires will forfeit a run or an entire dynamic event.

Comment: The intention of this rule is that sliding skirts or other devices that by design, fabrication or as a consequence of moving, contact the track surface are prohibited and any unintended contact with the ground which either causes damage, or in the opinion of the 'dynamic event organizers' could result in damage to the track, will result in forfeit of a run or an entire dynamic event

Rule T6.2 prohibits any part of the aero package from touching the ground. We need to ensure any skirts do not touch the ground while the car is stationary or scrape the ground while it is moving.

T9.2 Location – Front Mounted Devices

T9.2.1 In plan view, no part of any aerodynamic device, wing, under tray or splitter can be:

a. **Further forward than 700 mm (27.6 inches) forward of the fronts of the front tires**
b. **Wider than the outside of the front tires measured at the height of the hubs.**

T9.2.2 When viewed from the front of the vehicle, the part of the front wheels/tires that are more than 250 mm (9.8 inches) above ground level must be unobstructed by any part of the aerodynamic device, with the exception of any vertical surfaces (end plates) less than 25 mm in thickness.

NOTE: 9.2.1 and 9.2.2 apply with the wheels in the straight ahead position

T9.3 Location Rear Mounted Devices:

T9.3.1 In plan view, no part of any aerodynamic device, wing, undertray or splitter can be:

a. **Further rearward than 250 mm (9.8 inches) rearward of the rear of the rear tires**
b. **Further forward than a vertical plane through the rearmost portion of the front face of the driver head restraint support, excluding any padding, set (if adjustable) in its fully rearward position (excluding undertrays).**
c. **Wider than the inside of the rear tires, measured at the height of the hub centerline.**

T9.3.2 In side elevation, no part of the rear wing or aerodynamic device (including end-plates) may be higher than 1.2 meters above the ground when measured without a driver in the vehicle

T9.4 Location – General

T9.4.1 Between the centerlines of the front and rear wheel axles, an aerodynamic device (e.g. undertray) may extend outboard in plan view to a line drawn connecting the outer surfaces of the front and rear tires at the height of the wheel centers

T9.4.2 Except as permitted under T9.3.1, any aerodynamic devices, or other bodywork, located between the transverse vertical planes positioned at the front and rear axle centerlines must not exceed a height of 500 mm (19.7 inches) above the ground when measured without a driver in the vehicle. (Bodywork within vertical fore and aft planes set at 400 mm (15.75 inches) outboard from the centerline on each side of the vehicle is excluded from this requirement).

The Keep out zones of T2.1 (3) must not be infringed

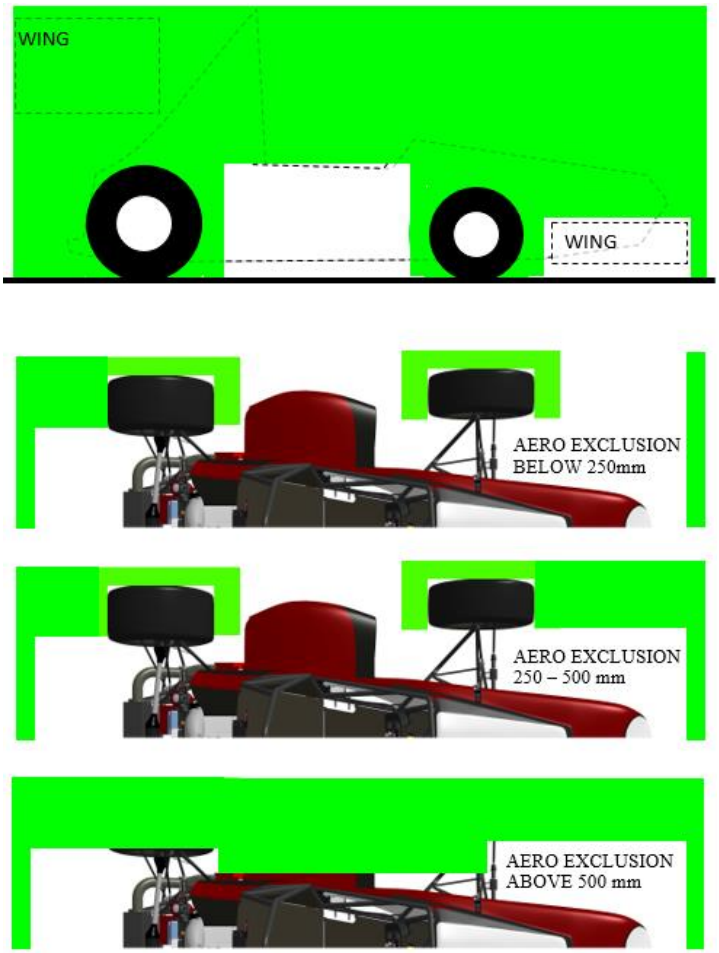

Figure 1.2: Complete aero location restrictions

Rules T9.2-T9.4 further restrict the location of aerodynamic devices. The front wing is limited to 700 mm forward of the front tires and may not obstruct the portion of the tires above 250 mm when viewed from the front. Side wings are limited to a height of 500 mm, except for portions less than 400 mm from the centerline of the car. The rear wing is limited to a height of 1.2 m and can be no further forward than the front face of the head restraint and no further rearward than 250 mm behind the rear tires. All aerodynamic devices must be inside the outboard edge of the

tires and the rear wing must be inside the inboard edge of the tires. These restricted areas are shown in green in Figure 1.2. This rule is also more restrictive than last year, and will require a large redesign of the aero package to fit within the new requirements. It will likely result in a significant decrease in downforce.

T9.5 Minimum Radii of Edges of Aerodynamic Devices

T9.5.1 All forward facing wing edges including wings, end plates, Gurney flaps, wicker bills and undertrays that could contact a pedestrian must have a minimum radius of 5 mm (0.2 inches) for all horizontal edges and 3mm (0.12 inches) for vertical edges (end plates). The 3/5mm radius requirements must be achieved with permanently affixed components and with specific design intent to meet this radius requirement.

For example, pushed on pieces of split tube relying on friction for retention are not a satisfactory engineering method of achieving the radii.

Rule T9.5 requires a minimum forward radius for aerodynamic devices. This will not be a problem for wings, but it will require a solution to be designed for endplates, skirts, gurney flaps, and any other similar parts.

T9.6 Ground Effect Devices
No power device may be used to move or remove air from under the vehicle except fans designed exclusively for cooling. Power ground effects are prohibited.

Rule T9.6 prohibits using power devices to move air under the vehicle. It does not prohibit using powered devices to move air in other places, such as a blown rear wing.

T9.7 Aerodynamic Devices Stability and Strength

T9.7.1 All aerodynamic devices must be designed such that the mounting system provides adequate rigidity in the static condition and such that the aerodynamic devices do not oscillate or move excessively when the vehicle is moving. In Technical Inspection this will be checked by pushing on the aerodynamic devices in any direction and at any point.

NOTE: The following should be seen as guidance as to how this rule will be applied but actual conformance will be up to technical inspectors at the respective competitions. The overall aim is to reduce the likelihood of wings detaching from cars whilst they are competing.

1. **If any deflection is significant, then a force of approximately 200N can be applied and the resulting deflection should not be more than 25mm and any permanent deflection less than 5mm.**

2. **If any vehicle on track is observed to have large, uncontrolled movements of aerodynamic devices, then officials will have the right to Black Flag the car for**

inspection and the car may be excluded from that run and until any issue identified is rectified.

Rule T9.7 provides strength requirements for aerodynamic devices. It does not provide specific required strength values; the only numbers given are guidelines. We should seek further clarification on this rule and how it will be enforced. Regardless of how this rule is implemented, we should build wings that are sturdy and reliable, but as lightweight as possible.

There are no rules which limit use of CFD simulation, wind tunnel testing, or on track testing. These will only be limited by our available time and resources.

1.3 Requirements

General Requirements

GFR uses Star-CCM+ for CFD studies. This program is sponsored, so it is available to the team at no cost. The team has a large amount of background knowledge related to the program. At least one CFD class (ME 567) is taught at OSU, using Star-CCM+. This means it would be very difficult to switch to using a different program. Therefore, the scope of this project will be limited to improving our model in Star-CCM+ and not exploring other CFD programs.

Aerodynamic Requirements

The aero package must produce high downforce, low drag, be lightweight, and be easy to manufacture. CFD will be used to help the aero design process by determining how much downforce and drag are produced by each design iteration. CFD is also useful to model other airflow characteristics, such as streamlines or pressure maps. These can be used to make educated decisions on how to improve the design. After the car is built, physical testing can be done to measure downforce and drag, and map pressure values. These measured values can be compared to CFD to evaluate the accuracy of the model.

Model Requirements

Sensitivity studies must evaluate parameters including, but not limited to mesh size, mesh type, prism layer thickness, number of prism layers, and turbulence models. These studies should be performed on airfoils at varying angles of attack (AoA). The results must be compared to published wind tunnel data. Simulations will also be performed on the full car model, and these results will be compared to physical testing results.

The model should accurately show, in descending order of importance, flow separation/stall angles, downforce values, and drag values. Flow separation is very important because it has a large detrimental impact on both downforce and drag. It is also believed that previous models

used by GFR do not accurately model the AoA at which flow separation begins to occur. If the model does not accurately determine flow separation, downforce and drag values will both be incorrect as well. Downforce is the next most important because points are much more sensitive to downforce than they are to drag. It is therefore more important for GFR to accurately model downforce than it is to accurately model drag.

The final model must also use a reasonably low amount of computational power. GFR currently has limited resources on which to run simulations. We do have access to a sponsored high-power computer, but we can no longer run simulations in computer labs overnight. GFR needs to run many different simulations, so each one should be reasonably fast. Therefore, the number of cells in the simulation should be small, and the simulation should converge quickly (i.e. with few iterations). In the past, simulations have converged in 8-10 hours on a high-performance desktop computer [3]. The new model should take a similar amount of time.

Team Requirements

The CFD model should be user-friendly and well documented so future members can use it easily. Simulation results should be stored in an easy-to-read spreadsheet format and simulation files should be stored on a team hard drive for future reference. This hard drive is stored near the grad student computers in Rogers 128.

2. Current State Analysis and Benchmarking

2.1 Current State Analysis

Past GFR projects have been devoted to improving CFD in various ways. Projects completed from 2011 to 2014 are summarized here.

2011 (Jasmin Birkenmaier [4])

The 2011 study began with the general goal of improving CFD through varying parameters within Star-CCM+. It started by using a polyhedral mesh (see Figure 2.1) and a k-omega turbulence model with an ideal gas approximation and a coupled flow solver. It used different mesh settings for individual parts (boundaries) but did not use volumetric controls.

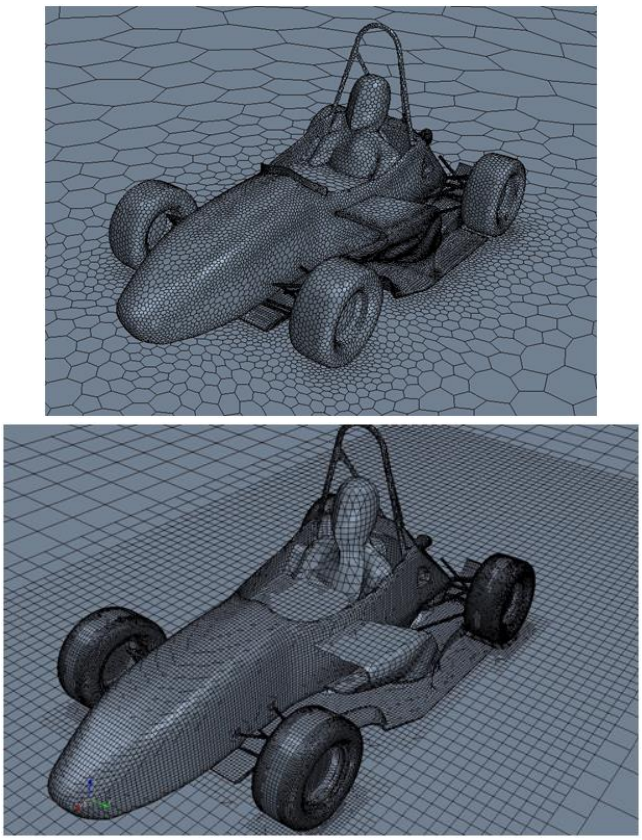

Figure 2.1: Polyhedral mesh (left) vs trimmer mesh (right) on GFR10 [3]

The study first tried to refine the mesh by changing mesh values on individual boundaries, and then through volumetric controls. Some of these volumes are shown in Figure 2.2. It did not successfully incorporate volumetric controls: they could not significantly improve mesh quality without adding too many cells. They next tried to improve the mesh by adding more prism layers. This improved the mesh quality without adding too many cells. Finally, the study tried using the k-epsilon turbulence model and segregated flow solver. It found that the segregated flow solver ran much faster than the coupled flow solver and that the k-epsilon model converged better and with fewer iterations than the k-omega turbulence model. These two physics models (segregated flow and k-epsilon) are currently used by GFR.

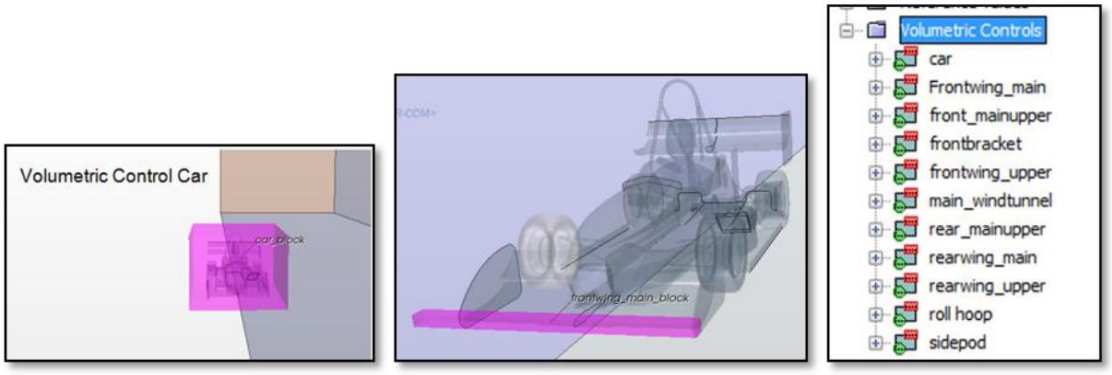

Figure 2.2: Volumetric controls used in 2011 [4]

This study was hindered by low computing power. It was not able to run models as complex as we can now; it was also only able to run a total of 14 simulations. It was able to explore the effects of different settings, but not compare many back-to-back results. It also did not make any comparisons between CFD results and measured data.

2012 (Denis Duschek [5])

The 2012 study performed wind tunnel testing and compared it to CFD results. The test apparatus and CFD model are shown in Figure 2.3. They took a single wing shape and varied the angle of attack and slot gap size. Their CFD simulations used the same settings recommended at the end of the 2011 study, with some minor changes to cell size and other similar parameters. They did not perform any tests with different CFD settings. This was the first time GFR was able to compare CFD results to a wind tunnel study.

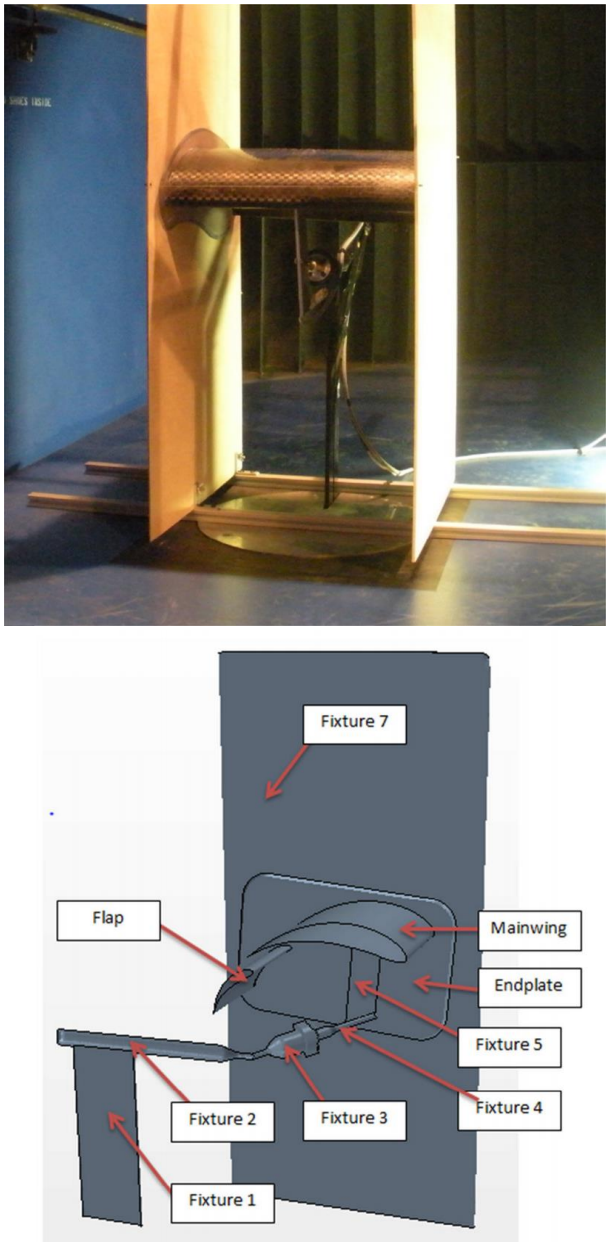

Figure 2.3: 2012 wind tunnel test apparatus and CFD model [5]

2013 (Ben Cox [3])

The 2013 study experimented with different meshes and volumetric controls, as well as comparing k-omega and k-epsilon turbulence models. Due to limits with computing power, they did not make many back to back comparisons with different settings in the same simulations. They created the Aero run/ran spreadsheet to organize results to make them easy to compare and find in future years. They corrected errors in the simulations by fixing the tire rotation axis and properly implementing contact prevention to improve the mesh. They also tried using the StarCAT5 module to directly import CATIA part files into Star-CCM+. This reportedly worked very well until the license began having problems. They also performed sensitivity studies on

various parameters on the car, such as angle of attack, front wing ride height, and yaw. Coast down testing was used to get physical testing data.

2014 (Curtis Peterson [6])

The 2014 study again compared wind tunnel testing to CFD data. This time, slot gap testing was performed on a triple-element wing in the OSU wind tunnel. The CFD model mimicked the wind tunnel geometry and used a trimmer mesh and k-omega turbulence (See Figure 2.4). The model had an appropriately thin (4 mm) prism layer and used separate volumetric controls for parts and wake refinement. These models were selected based on the recommendation of a CD-adapco webinar [7]. There was no experimentation performed with different settings.

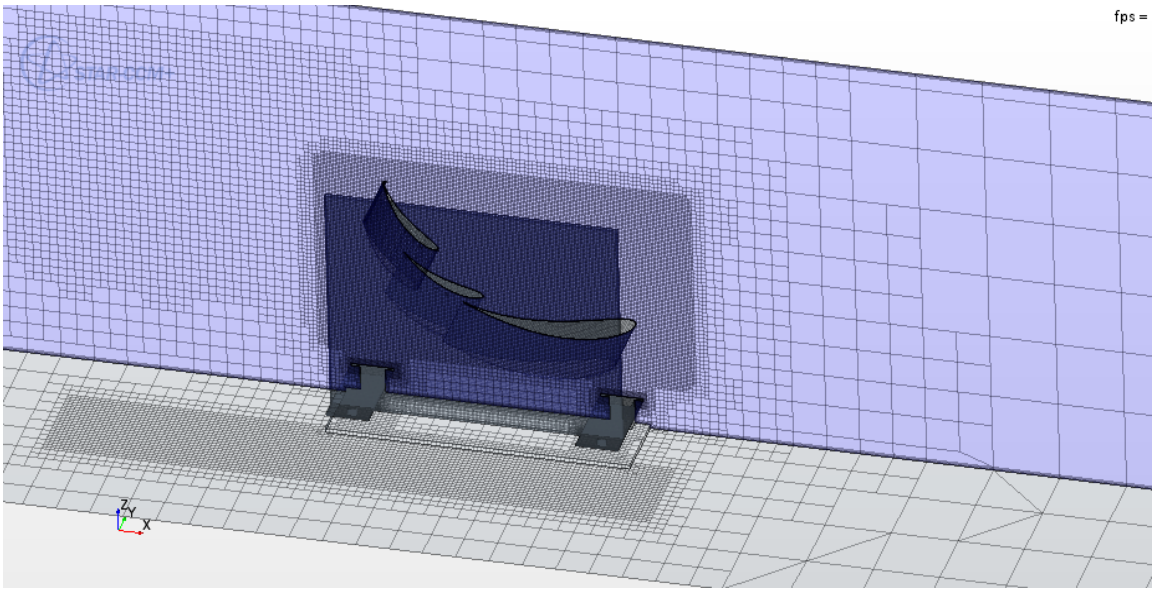

Figure 2.4: Curtis' wind tunnel model [6]

Separate from Curtis' study, full car simulations were performed with a trimmer mesh and a 1 m base cell size. Volumetric controls (VCs) were used to refine the mesh around the full car, as well as additional VCs for finer meshes around aerodynamic elements. Within the aero VCs, prism layers had a minimum thickness of 10 cm and two layers. This resulted in blocky prism layers (shown in Figures 2.5 and 2.6) which sometimes did not cover the entire wing. It was theorized that, while unusual in appearance, these layers somewhat accurately modeled flow separation. Other models were thought to predict flow separation at too low angles of attack. However, wings too close to the ground or too close to other wings failed to generate prism layer in those areas, leading to a probable loss of accuracy. K-epsilon turbulence was used because it tended to converge quickly and without major oscillations in the solution. This model was the starting point for 2015 CFD.

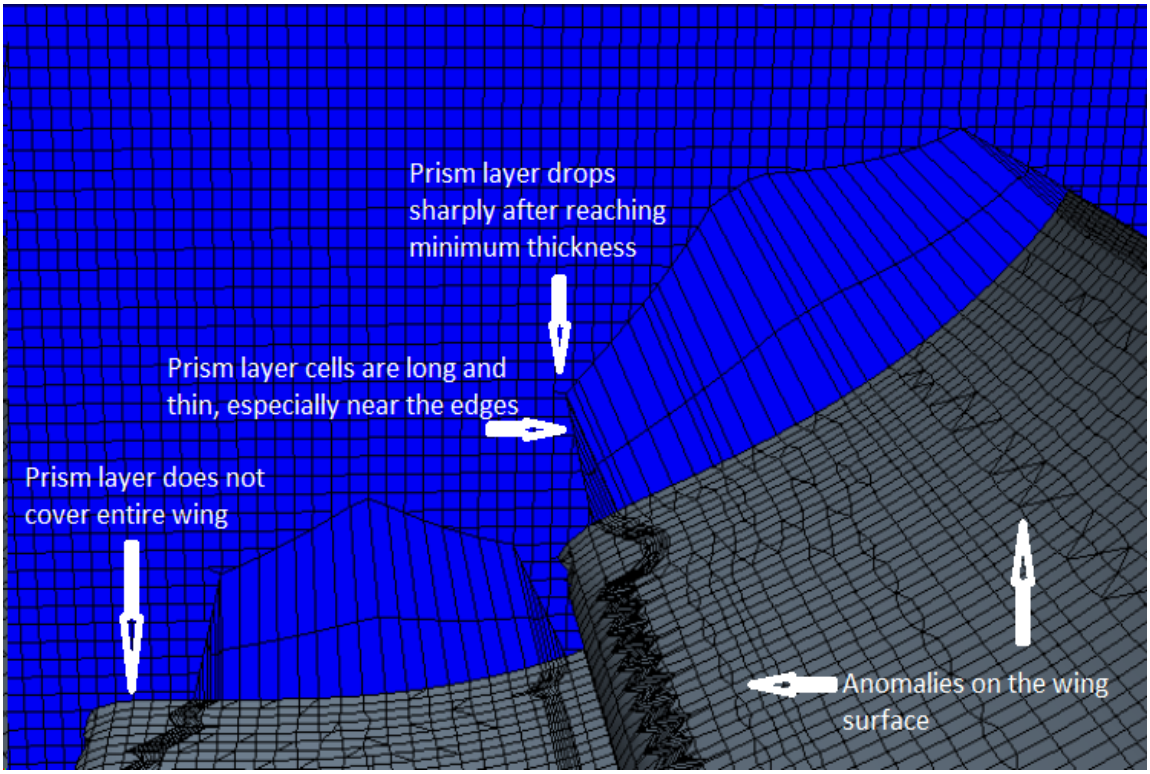

Figure 2.5: 2014 prism layers

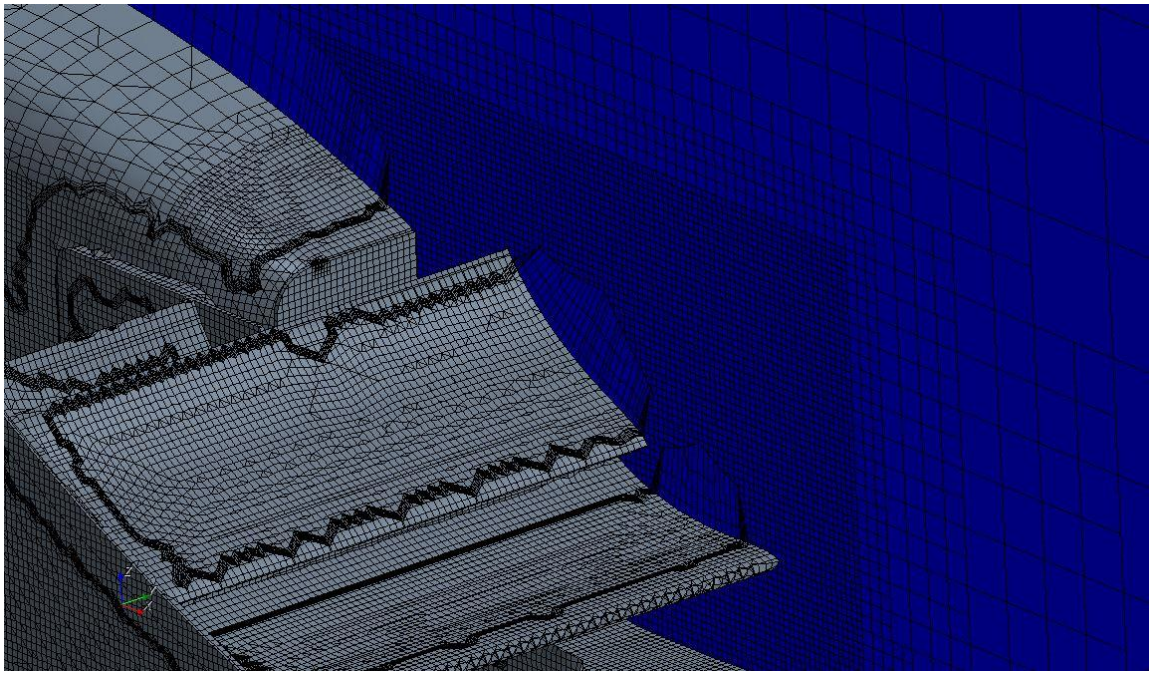

Figure 2.6: 2014 front wing mesh [6]

SWOT Analysis

Strengths:

- Experience with CFD

  In past years, most OSU seniors have worked on CFD projects with little or no prior experience with Star-CCM+. I am already familiar with the program, so I will not have to spend as much time learning
- Access to high-performance server

  We currently have a sponsorship with Sabalcore which allows us to run simulations very quickly on their server.
- Wind tunnel access

  There is an OSU wind tunnel which GFR has been able to get access to.

Weaknesses:

- Physical testing experience

  I have no experience working with Motec or wind tunnel testing sensors. I will have to learn how these work and avoid using them improperly, which could produce misleading results.
- OSU Wing tunnel size

  The OSU wind tunnel is too small to test full-size wings without interfering with the wake. It also cannot reach wind speeds high enough to test small-scale models with dynamically similar conditions.

Opportunities:

- Access Daimler wind tunnel

  The Daimler wind tunnel could be used with the entire car. GFR has been able to get access in the past. The biggest issue is logistically preparing the car and test fixture.
- Star-CCM+ Individual License

  An individual license for a personal computer may be acquired from CD-adapco. This would be particularly useful for simulations with a single airfoil which converge fairly quickly (a multi-core operation) but still take a large amount of time to generate meshes (a single-core operation).

Threats:

- Delays in manufacturing/assembly

  Data acquisition for aero is lower priority than having a reliable, running car. In the 2014 season, strain gages and pressure taps were not installed in time to get data before Michigan. This issue may be solved by having a dedicated data acquisition project this year.

2.2 Benchmarking

Converting Aerodynamic Parameters to Points

Drag and downforce are the two parameters found with CFD that have a direct correlation to points received at competition. These correlation values were found using a student built lap simulation [1], and are tabulated in Table 2.1. These can be used to objectively determine which of any two designs is better. For example, a design change that adds 10 N of downforce, doesn't change drag, and adds 1 kg of mass to the eCar would add a net 1.938-1.339=0.599 points. From this table, we can see that downforce is more point-sensitive than drag in all competitions. Therefore, a design change which adds an equal amount of downforce and drag could still be beneficial, if it did not negatively impact mass or other parameters. The point values for downforce and drag are automatically calculated for designs in the aero run/ran spreadsheet [8], but the sheet does not consider mass or CG values at this time. Mass point calculations could be added fairly easily.

Table 2.1: Converting parameters to points [1]

	cCar Points		eCar Points	
Parameter	FSAE	FSG/FSA	FSAE	FSG/FSA
1 kg mass	-1.503	-1.973	N/A	-1.339
1 N-m torque	3.000	2.049	N/A	0.015
10 mm CG height	-3.242	-4.457	N/A	-3.209
10 N downforce	1.594	2.064	N/A	1.938
10 N drag	-1.382	-1.535	N/A	-0.235

Existing CFD Model Parameters

GFR10

Reference file: full-car_5-31-10_a-arm_clearance_final_no-gurn_50mph.sim

Mesh:	Trimmer
Cell count:	5.6 million
Base size:	9 mm
Prism layers:	5 (3 mm total thickness)
Surface size:	min: 25% base
	target: 100% base
Contact prevention:	All parts included; in six separate sets

Physics model: K-epsilon

Solver:	Coupled
Gas model:	Ideal
Floor type:	Slip
Other notes:	Modeled monocoque interior, engine (see Figure 2.7)
	Did not model sidepod, suspension, roll hoop
	Did not use volumetric controls
	Used smaller wind tunnel than is used now (12.5 x 3.75 x 3.75 [m])
	Car located near front of wind tunnel (See Figure 2.8)
	Despite "full-car" label, it is a half-car simulation

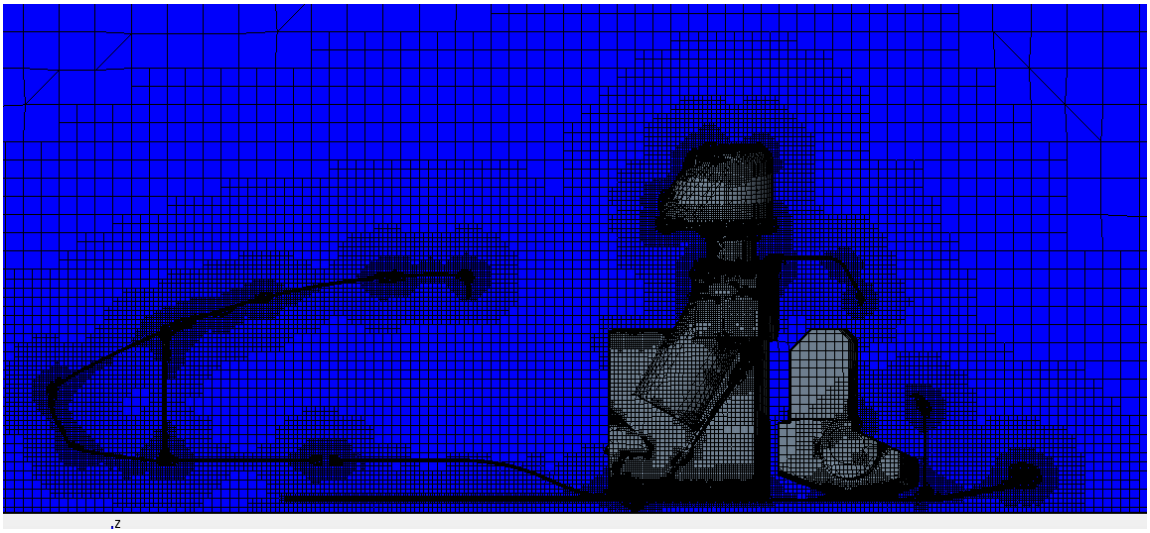

Figure 2.7: The GFR10 model included the interior of the chassis

The GFR10 model had several issues which have been corrected in later models. It modeled the interior of the chassis, which greatly increased the cell count, and used a wind tunnel model that was much smaller than the CD-adapco recommended size of 5 body lengths upstream, 10 body lengths downstream, and 5 body widths to the side and above [9]. It also used a coupled flow solver, which increases solving time and is not necessary for low speed flows.

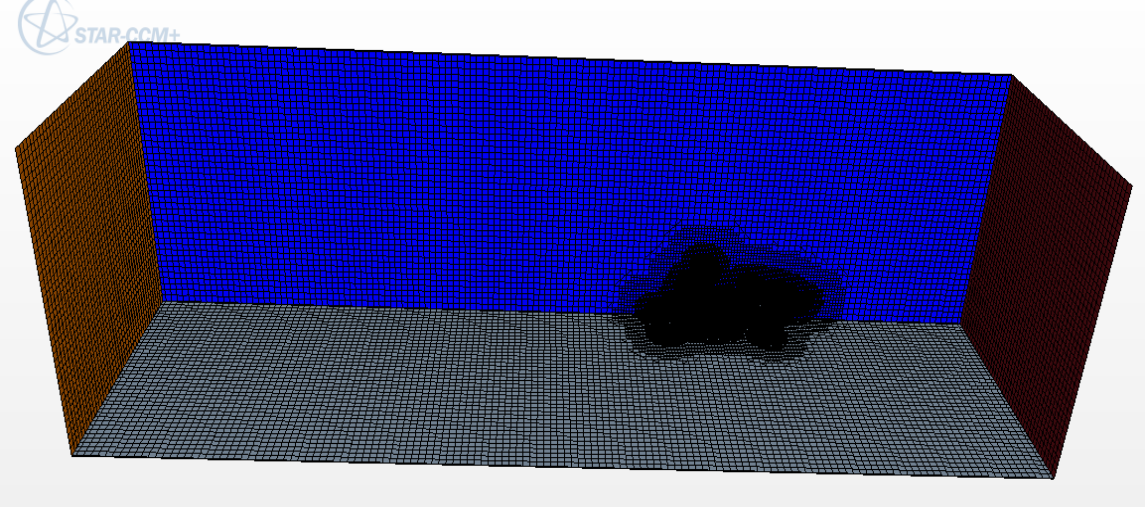

Figure 2.8: The GFR 10 model used a small wind tunnel with the car near the front

GFR11

Reference file:	GFR11_FullCar_BaselineAero_FW(D7)_UT(E2)_RW(C3)_SP(H3+Rad)_ WingBrackets(SolidFrontBracket)_NewEndplates_65kph.sim
Mesh:	Polyhedral
Cell count:	4.4 million
Base size:	1 m
Prism layers:	5 (50 mm total thickness)
Surface size:	min: 2% base target: 100% base
Contact prevention:	All parts included; in >15 separate sets

Physics model: K-epsilon

Solver:	Segregated
Gas model:	Ideal
Floor type:	Moving

Other notes:	Did not use volumetric controls Used large wind tunnel (43.2 x 7.5 x 5 [m]) with car located ⅓ from front Despite "full-car" label, it is a half-car simulation

The GFR11 model increased the size of the wind tunnel and switched to a segregated flow solver. It also changed to a polyhedral mesh and a moving floor model. However, it continued to use the ideal gas model and not use volumetric controls.

GFR12

Data not available.

The GFR12 CFD files are not available for benchmarking. In these models, the wheels were rotating about the global origin, rather than the wheel center. This added about 50N of

downforce. This should be considered when reviewing data from 2012.

GFR13

	Reference file: GFR13_Half_Body_FW_2.sim
Mesh:	Trimmer
Cell count:	2.6 million
Base size:	1 m
Prism layers:	5 (500 mm total thickness)
Surface size:	min: 2% base
	target: 100% base
Contact prevention:	All parts included; in one set
Volumetric controls:	Car, Front Wing, Rear Wing, Undertray

Physics model: K-epsilon

Solver:	Segregated
Gas model:	Incompressible
Floor type:	Moving

Other notes: Prism layers were too thick to form correctly in some places

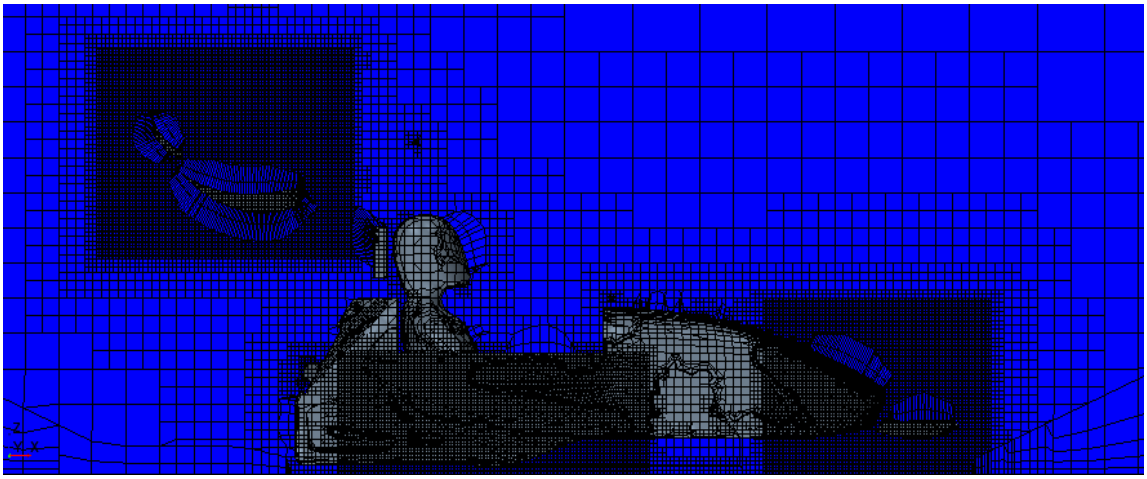

Figure 2.9: Volumetric controls and prism layers in GFR13 model

Most settings in the GFR13 model were copied from 2012; some were changed based on a CD-adapco webinar. This model successfully used volumetric controls for the first time. It also thickened the prism layer, and in some places volumetric controls reduced it to just two layers thick. This resulted in the long, narrow cells and blocky prism layers shown in Figure 2.9. These prism layers were too thick to form in some areas, such as between wing elements or below the front wing.

GFR14

	Reference file: GFR_14_Half_Body_SP_1.18_Trimmer.sim
Mesh:	Trimmer
Cell count:	3.6 million
Base size:	1 m
Prism layers:	5 (500 mm total thickness)
Surface size:	min: 2% base
	target: 100% base
Contact prevention:	All parts included; in one set
Volumetric controls:	Car, Front Wing, Rear Wing, Undertray, Splitter

Physics model: K-epsilon

Solver:	Segregated
Gas model:	Incompressible
Floor type:	Moving

Other notes:	Same prism layer issues as GFR13
	Added porous region to measure mass flow rate through coolers

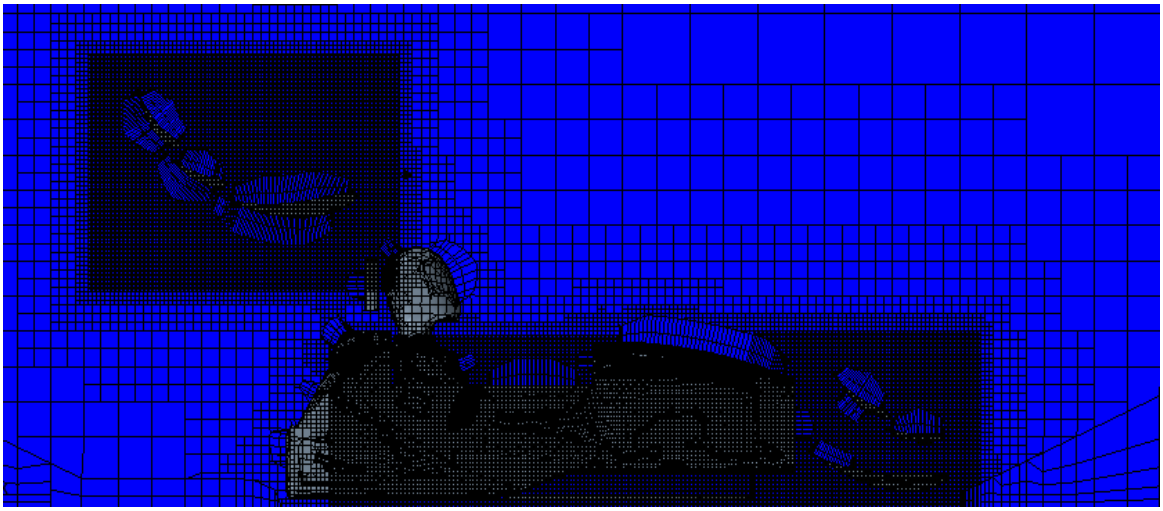

Figure 2.10: GFR14 model volumetric controls and prism layers

The GFR14 model had the same prism layer problems as GFR13. These are especially evident on the front wing in Figure 2.10. It extended the volumetric controls to better capture the side wing and sidepod, and added an additional volumetric control for the splitter. This model also added a porous region for the cooler, which allowed mass flow rate through the coolers to be measured.

Time to Converge

GFR has limited computing resources available to run CFD simulations. It is therefore important that simulations converge relatively quickly. This can be broken into two parts: time per iteration, and iterations to converge. Time per iteration is generally relative to cell count, and can also depend on the physics models used and the mesh type. Iterations to converge seems to be dependent on many variables, and previous GFR models have shown it to be heavily influenced by the physics model. Convergence time was measured using the representative simulations noted above. To standardize results, all of these simulations were run on identical computers in Rogers 336 (4 cores on Intel Xeon E3-1240 V2 processor; 12 GB ram). Three quantities were measured from each simulation: time to mesh (includes both surface and volume meshes), time to complete first 1000 iterations, and iterations to converge. Convergence was defined by the Total Downforce monitor varying by less than 1 N for 200 iterations. This is roughly how GFR determines if a simulation is converged; however, there is not a standardized definition currently. From this data, Time per step was calculated as (1000 step time)/1000. Extrapolated convergence time was calculated as (Mesh time)+(Time/step)*(steps to converge). The results are shown below in Table 2.2.

Table 2.2: Convergence Time Study Results

Model	Mesh time (s)	1000 step time (s)	Time/step (s)	Steps to converge	Extrapolated convergence time (hrs)
GFR10	N/A	N/A	N/A	N/A	N/A
GFR11	1440	18144	18.1	1900	10.0
GFR12	N/A	N/A	N/A	N/A	N/A
GFR13	544	9320	9.3	2300	6.1
GFR14	1053	13855	13.9	2200	8.8

The GFR10 model would not generate a mesh. It did not crash or show any errors, but did not make any progress after 20 hrs. When trying to run the simulation with an already existing mesh, it also failed to run in a reasonable amount of time. It attempted to use 24 GB of ram, double what was available. Data is not available for the GFR12 model because simulation files are no longer available.

Mesh Quality Parameters

The wall y+ value is a non-dimensional measure of distance from a part boundary, or wall [10]. It is defined as:

$$y^+ = \frac{yu^*}{v}$$

where y is the distance normal to the wall from the wall to the centroid of the near-wall cell, u* is a reference velocity, and *v* is the kinematic viscosity [11]. The user can change this value by changing the thickness of the first prism layer to alter y. Star-CCM+ can automatically calculate y+ values for all surfaces, as shown in Figure 2.11.

The y+ value is useful for characterizing the near-wall area which is significantly affected by viscosity. This can be divided into three regions: the viscous sublayer (y+ < 5), the buffer layer (5 < y+ < 30), and the log-law (fully turbulent) layer (y+ > 30~60) [12]. Based on experiments by Salim and Cheah, a reasonably accurate solution can be obtained with a near wall cell y+ value in the viscous sublayer or log-law region. They suggest avoiding the buffer layer, as turbulence models do not yet accurately account for it. Their final recommendation is a y+ value slightly larger than 30 for near wall cells. This uses fewer cells than a y+ value in the viscous sublayer, and based on their experiments, it results in an equally accurate solution. It is important to use the correct wall treatment model: wall function for y+ ≈ 30, or near-wall function for y+ < 5 [12].

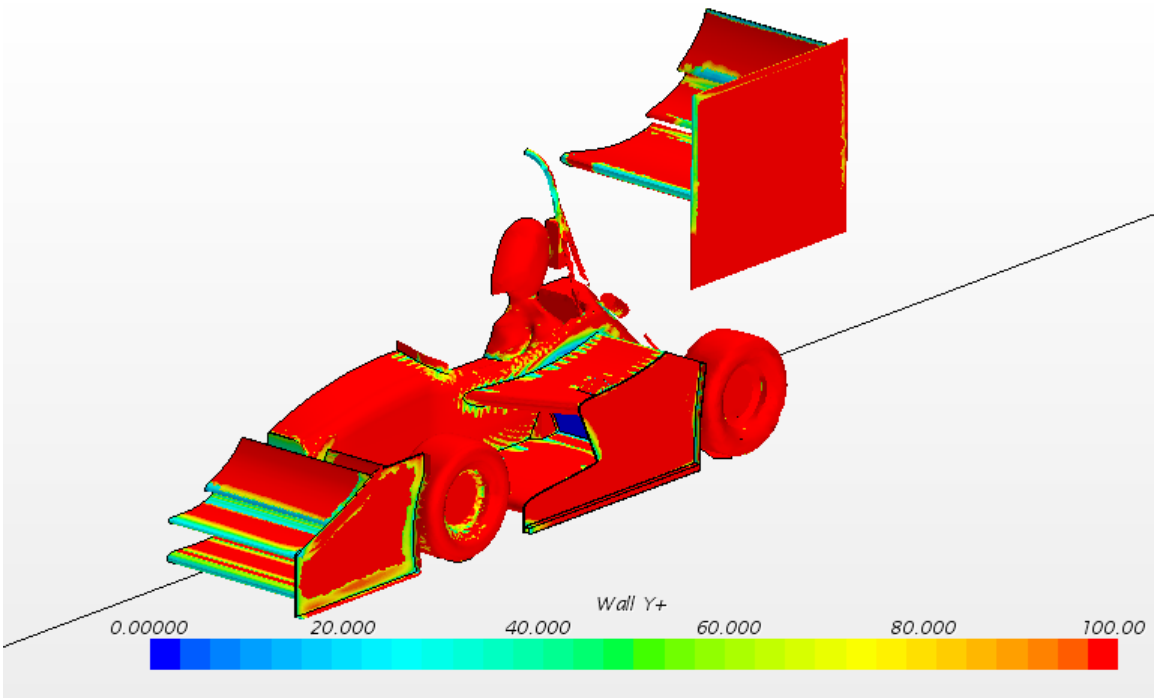

Figure 2.11: Wall y+ values on GFR14 model

In almost all locations on the car, these values are much larger than 30. In particular, wherever the elongated prism layer cells appear, the y+ values are very high. Using settings recommended

in CD-adapco's video tutorials [13] may help this problem.

3. Design Analysis

There are too many parameters that can be changed within Star-CCM+ to evaluate the effect of each one. Listed below are the models and settings believed to be most important for creating an accurate and efficient CFD model for a Formula SAE car. Each of these could be used in comparison or sensitivity studies to determine the settings for the best results.

The goal of this study is to improve the CFD model to more accurately find the aerodynamic parameters most important to the team: flow separation angle, downforce, and drag. It is also important to not increase the computational time required to run a simulation. The designs proposed here seek to improve the accuracy of the aerodynamic parameters while maintaining or reducing computational time.

3.1 Volumetric Controls

Volumetric controls are used to decrease the cell size in important areas of the model, such as around wings. Currently, only rectangular volumetric controls are used in the GFR model. There are several potential improvements which could be made to the volumetric controls.

1. Cut corners

   Currently, rectangular volumetric controls are used even when this shape doesn't make sense. Cell count could be reduced by removing unnecessary parts of volumetric controls, such as the upper front corner of the front wing volumetric control, as shown in Figure 3.1. Tests should be performed to ensure this does not reduce accuracy.

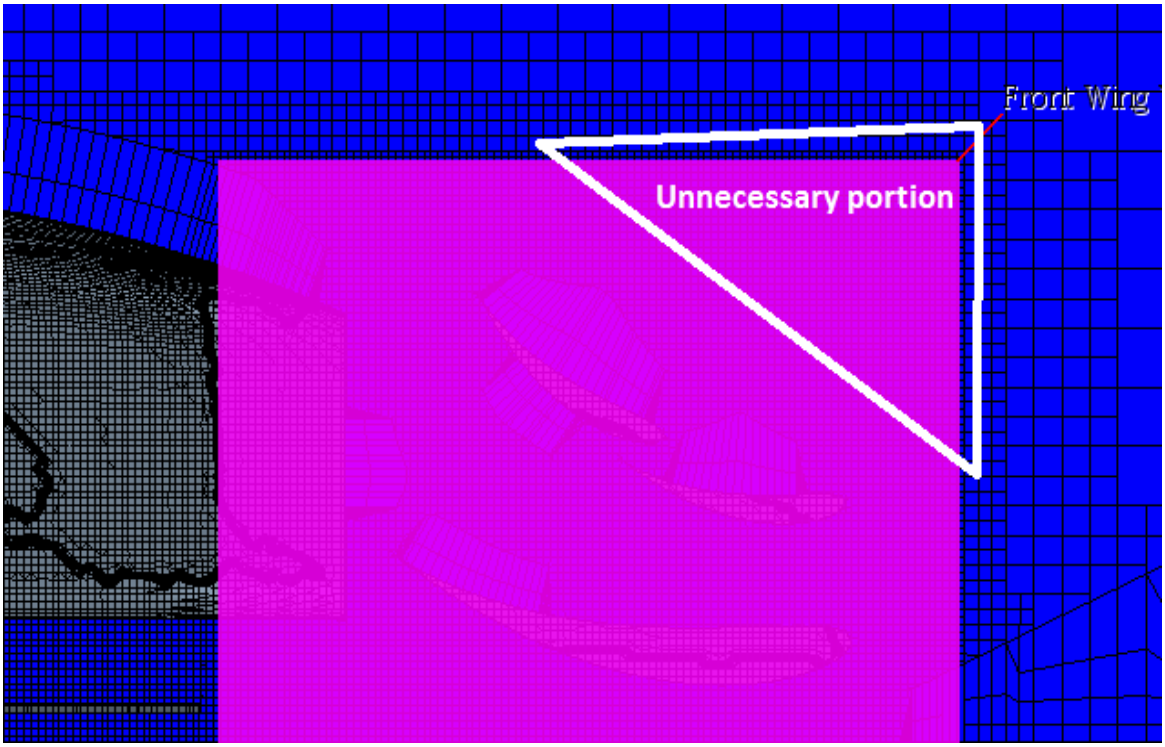

Figure 3.1: Cutting corners off the 2014 front wing volumetric control

A quick test removing the portion marked in Figure 3.1 in the GFR2014 model reduced cell count by 329,000, or 9.1%.

2. Wake refinement

Wake refinement is used to improve the mesh in the wake behind a part, shown in Figure 3.2. This is important to correctly capture flow separation. Wake refinement can be accomplished in several ways. It can be done manually with volumetric controls, or Star-CCM+ is able to automatically perform wake refinement on parts contained in sets, much like contact prevention sets [11]. It is possible that accuracy could be increased by refining the mesh in wake regions. It is also possible that the automated function could do a better job of this than manually moving the volumetric controls, or it could work poorly. Tests should be performed to see the impact of each.

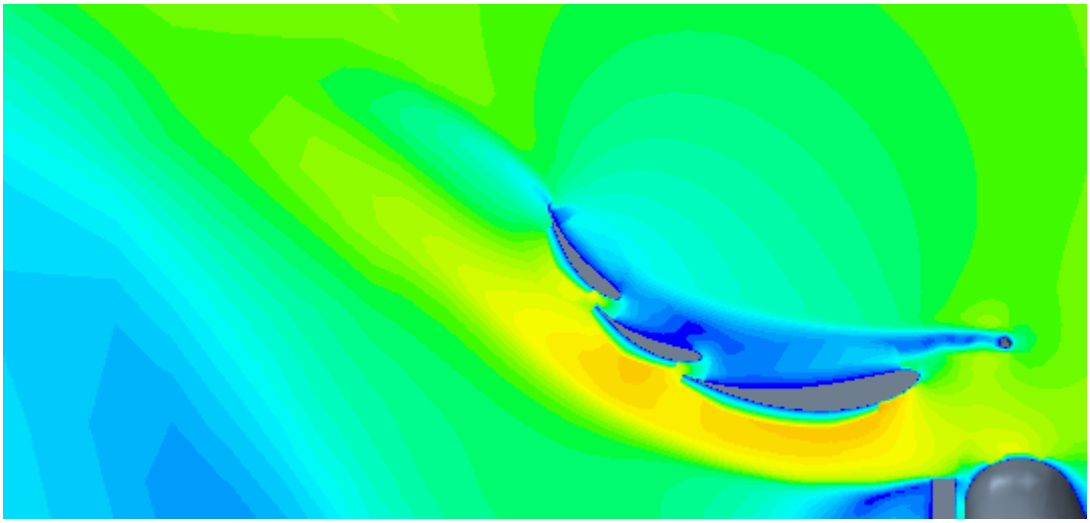

Figure 3.2: Wake behind the rear wing in GFR14

3. Per-part settings

   Currently, we use volumetric controls to both refine the mesh on the part surface and nearby the part, such as the wake. It is also possible to change all of the same settings (such as surface mesh size, prism layer, etc.) on a per-part basis. This could give more precise control while eliminating the wasted cells described in part 1. Used in conjunction with the automatic wake refinement tool, this could produce the same effect as volumetric controls, while strategically positioning the cells to reduce cell count. This would likely require more work for the user, but after an initial setup, it might be possible to use it easily.

4. Leading/trailing edge refinement

   The leading and trailing edges of the wing are the most important parts to model for accuracy. Therefore, the most efficient mesh would have higher density cells in these regions than in other parts of the wing [14]. Volumetric controls can be used in these areas to accomplish this. However, this would require a large amount of time from the user to position these correctly for each new design.

3.2 Mesh Type

Mesh models are used to transform CAD geometry into a volume mesh that the flow equations can be solved on. There are a few different options available in STAR-CCM+. In each mesh model, many settings such as base size and surface curvature can be adjusted.

1. Polyhedral Mesh

   The polyhedral mesh uses many-faced cells, as shown in Figure 3.3. It is able to accurately mesh with fewer cells than other mesh types [11]. GFR should perform studies to objectively compare time to convergence for polyhedral vs. trimmer meshes, in terms of physical time and iterations. We should also

determine what impact mesh type has on the downforce and drag results, and compare these to experimental data.

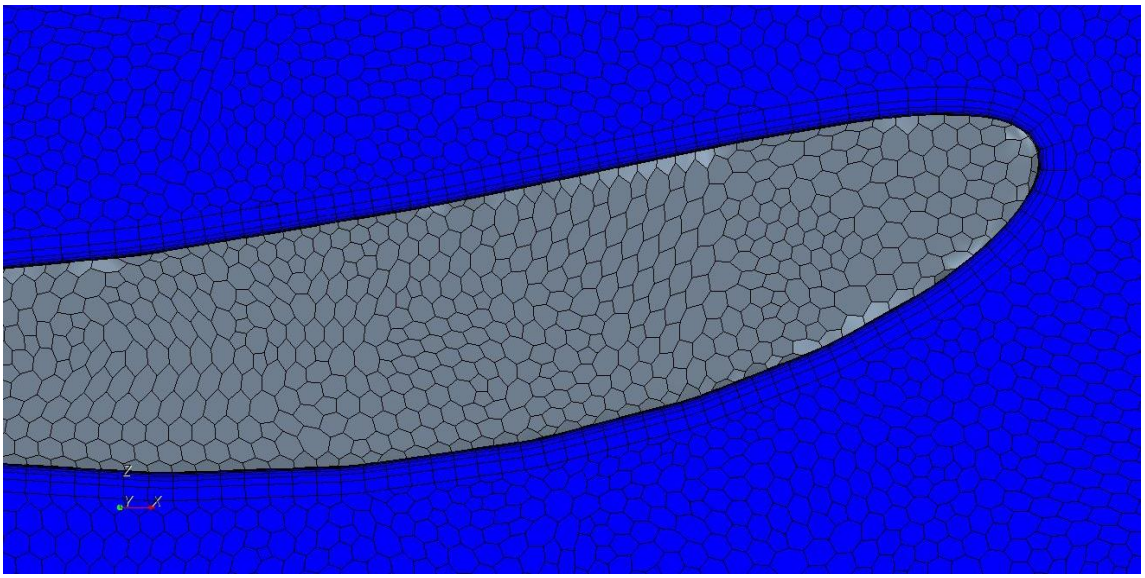

Figure 3.3: Polyhedral mesh [6]

2. Trimmer mesh

   The trimmer mesh uses hexahedral cells for the main mesh, and cuts corners off of hexahedra to fit curved surfaces, as shown in Figure 3.4. The trimmer mesh excels at rapidly moving between large and small cell regions [11].

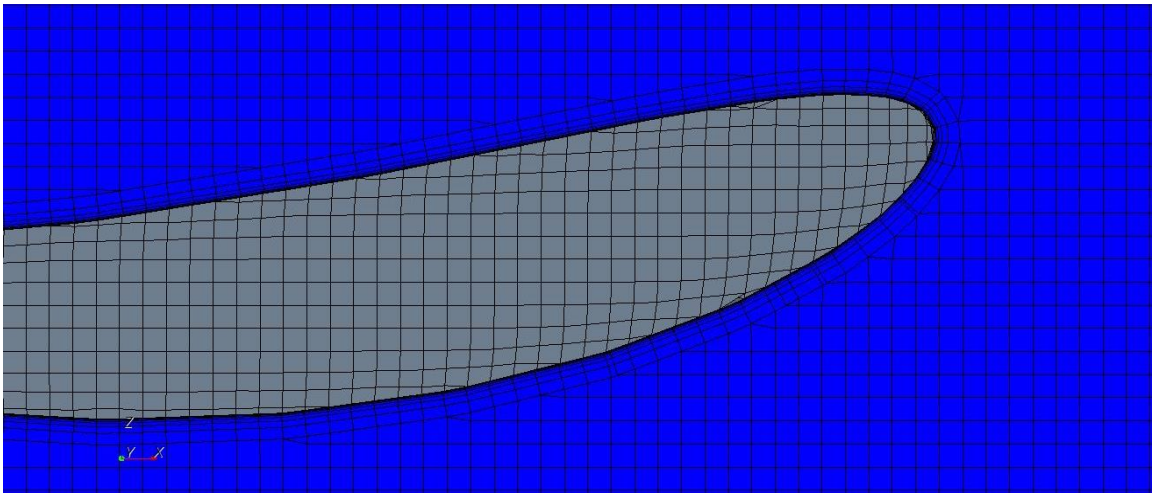

Figure 3.4 Trimmer mesh [6]

3. Tetrahedral mesh

   Tetrahedral mesh has been concluded to be worse than the other two listed mesh types, both in terms of accuracy and cell count. It is considered obsolete, and should not be investigated any further [6].

3.3 Prism Layer

The prism layer is made of specially shaped cells near part surfaces which allow the boundary layer to be modeled more accurately. It has several simple parameters which can be altered, such as thickness and number of layers. Other parameters can be altered to better fine-tune how prism layers behave in places such as sharp corners and between two nearby surfaces. These parameters include:

- Gap fill percentage: the maximum distance a prism layer can extend into a space between two surfaces, expressed as a percentage of the total distance.
- Minimum thickness percentage: the minimum thickness a prism layer can be before it is removed entirely, expressed as a percentage of maximum thickness.
- Layer reduction percentage: the minimum thickness a prism layer can reach before the number of layers is reduced, expressed as a percentage of maximum thickness
- Concave angle limit: in corners less than this angle, prism layer thickness will be reduced as it approaches the corner to avoid large aspect-ratio cells [11]. This effect is illustrated in Figure 3.5.

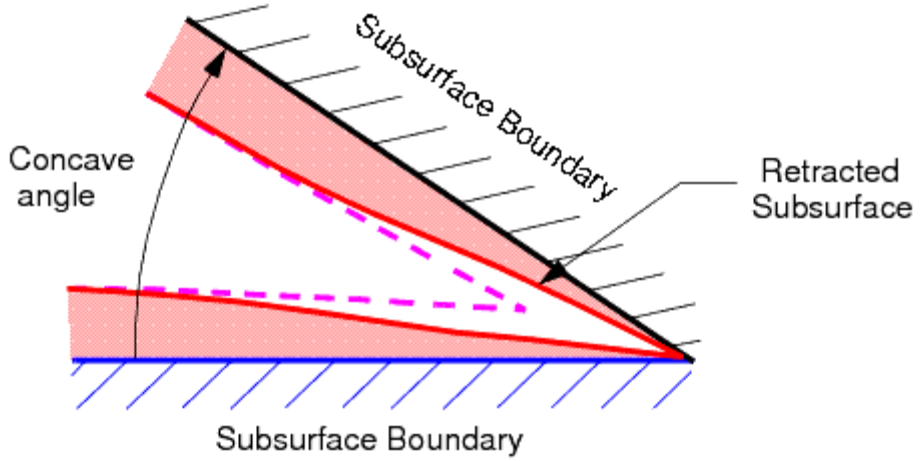

Figure 3.5: Concave angle limit [11]

- Convex angle limit: at exterior corners less than this angle (such as a trailing edge), the prism layer thickness will be reduced to give a higher quality prism mesh [11]. This effect is shown in Figure 3.6.

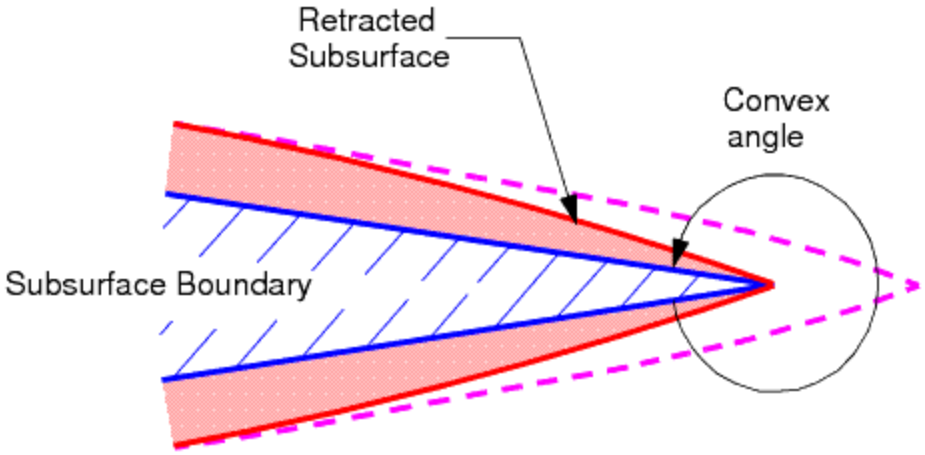

Figure 3.6: Convex angle limit [11]

These parameters should be experimented with to see how they affect the prism layer and which configuration produces the best results. Results can be measured with y+ value and downforce/drag comparisons to experimental data.

3.4 Physics Model

The physics model contains the actual equations used to solve the flow characteristics. There are a few main models available in Star-CCM+.

1. k-epsilon turbulence

   The k-epsilon turbulence model is useful for low-speed flows, making it appropriate for FSAE models [11]. Past use by GFR has shown it to converge quickly and smoothly.

2. k-omega turbulence

   The k-omega turbulence model is recommended by CD-adapco for formula student models as more accurate than k-epsilon for low speed flows [7]. It has been used by GFR in the past, and shows a tendency to converge slower and with more oscillations than the k-epsilon model. It is very sensitive to initial boundary conditions, but can model flow separation better than other models. Because it is so sensitive to initial conditions, sometimes a k-epsilon model is used to converge on a solution, and then that solution is used with a k-omega model to achieve a final result [15].

3. Spalart-allmaras

   The spalart-allmaras model performs better with high speed flow than either k-omega or k-epsilon. It generally does not model separation or recirculating flow very well [15]. Both of these characteristics make it a poor choice for FSAE models.

3.5 Wind Tunnel

There are a few miscellaneous changes that could be made to the wind tunnel model.

1. Floor model

   The floor can be modeled as either a slip wall or a moving wall. GFR has done each in the past. We do not currently know which more accurately models the flow beneath the car. A moving wall is more representative of the ground moving beneath the car, but may cause issues with prism layer interference between the floor and the lower surface of the car. A slip wall will not have a prism layer, but may not be an accurate physical representation.

2. Wind tunnel size/car location

   CD-adapco recommends a wind tunnel sized 5 body lengths upstream, 10 body lengths downstream, and 5 body widths to the side and above [9]. In the current model, the car is located about halfway down the wind tunnel. Different locations could be experimented with.

4. Design Selected

The selected design changes will be simulated and compared against experimental data using a wind tunnel model and an airfoil with published results. The simulated downforce and drag values will be compared to wind tunnel results to determine accuracy. For this model, the NACA 6409 airfoil was selected from the publication by Selig et al. [16]. Several of the best results from the wind tunnel study will be run in the half car model and compared with experimental data from GFR testing.

4.1 Rationale for Selection

The single airfoil model is used because it is much simpler than the full car, so many design iterations can be compared very quickly and analyzed easier. The NACA 6409 airfoil (shown in Figure 4.1) was selected because it has a large amount of published data readily available and it is similar to the Joukowski profiles used on the GFR cars. Both are used for low-speed aerodynamic applications. It has lower thickness (9% vs 12%) and camber (6% vs 10%) than the GFR profiles, but it is the closest match found. The wind tunnel model includes all major parts present in the actual wind tunnel to improve accuracy.

Figure 4.1: NACA 6409 Airfoil

The chosen tests were selected because they are believed to be the most likely to improve the accuracy of the simulation in the areas of downforce, drag, and flow separation, based on the suggestions from CD-adapco and other sources, as noted in section 3. Improving accuracy in these areas will allow us to design a better aerodynamic package and earn more points at competition. A few tests were also chosen to improve simulation speed. Improvements in speed could allow more simulations to be run, or could offset changes that improve accuracy, but add time.

4.2 Technical Specification

To match the Selig et al. experiment, the wind tunnel model will use a NACA 6409 airfoil with chord length 12 in and span 33 ⅝ in. The wind tunnel is 8 ft. long, 2.8 ft. high by 4 ft. wide at the entrance and increases in width by 0.5 in at the exit. The endplates are ⅜ in thick, 6 ft. long, and the same height as the wind tunnel [16]. A photograph of the actual wind tunnel is shown in Figure 4.2. The modeled wind tunnel will take advantage of the wind tunnel symmetry and include only one half, as shown in Figure 4.3.

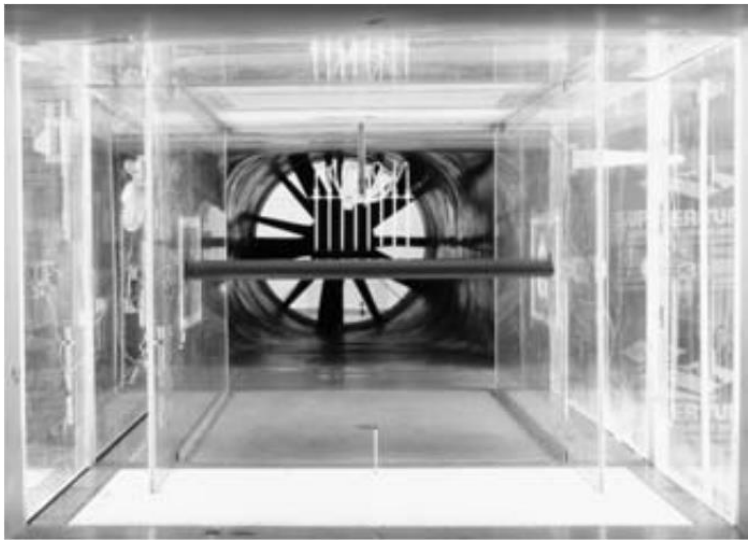

Figure 4.2: Actual wind tunnel [16]

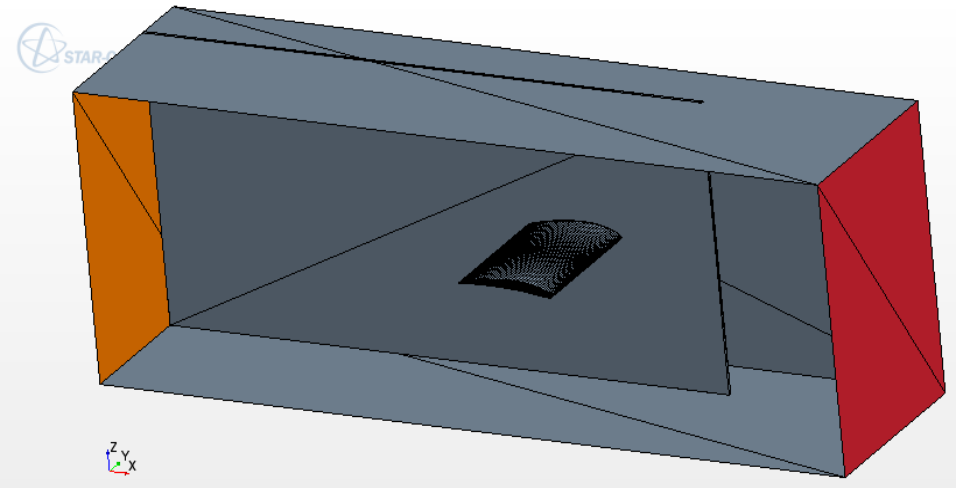

Figure 4.3: Wind tunnel model

The simulations listed in Table 4.1 will be run in the single-airfoil model. The baseline (BL) will use the same settings used in the 2015 half-car simulations. Most other simulations will start with the baseline and make a single alteration. The parameters changed in these simulations are quantified where possible. Some will require several tests to determine reasonable values for parameters GFR has not experimented with in the past, such as layer reduction percentage or convex angle limit. Because of this, additional simulations will be added as testing progresses.

Table 4.1: Single Airfoil Simulation Specifications

#	**Name**	**Description**
BL	Baseline	Standard 2015 settings
VC1	VC scaling 1	BL with VC covering just wing
VC2	VC scaling 2	VC1 with VC scaled 1.5x
VC3	VC scaling 3	VC1 with VC scaled 2x
VC4	VC extension rear	BL with VC scaled 1.5x in x direction; extends rearward
VC5	VC extension front	BL with VC scaled 1.5x in x direction; extends forward
VC6	VC extension top	BL with VC scaled 1.5x in z direction; extend up
VC7	VC extension bottom	BL with VC scaled 1.5x in z-direction; extend down
VC8	Wake refinement	BL with wake refinement turned on
VC9	Surface refinement	BL with no VC; use surface refinement instead
VC10	Wake/surface refinement	VC9 with wake refinement from VC8

VC11	Edge refinement	BL with additional VCs for trailing/leading edge refinement
M1	Polyhedral mesh	BL with polyhedral mesh
PL1	Prism layer 1	BL with 3 prism layers on wing
PL2	Prism layer 2	BL with 5 prism layers on wing
PL3	Prism layer 3	BL with 7 prism layers on wing
PL4	Prism layer 4	BL with 10 prism layer on wing
PL5	Prism layer thickness 1	BL with prism layer thickness 50% smaller
PL6	Prism layer thickness 2	BL with prism layer thickness 50% larger
PL7	Prism layer thickness 3	BL with prism layer thickness 100% larger
PL8	PL convex angle limit	BL with convex angle limit turned on
PL9	PL concave angle limit	BL with concave angle limit turned on
PL10	PL minimum thickness % 1	BL with minimum thickness percentage increased
PL11	PL minimum thickness % 2	BL with minimum thickness percentage decreased
PL12	Layer reduction % 1	BL with layer reduction percentage increased
PL13	Layer reduction % 2	BL with layer reduction percentage decreased
PH1	k-omega physics model	BL with k-omega physics model
PH2	k-omega physics post	Iterate BL solution with k-ω model

Abbreviations used in this table:

BL-baseline
VC-volumetric control
M-mesh
PL-prism layer
PH-physics

Some simulations will require the half car model to provide useful data. These are listed in Table 4.2 below. Cutting VC corners requires a half car model to quantify what benefit it will have with the different areas of the car. The polyhedral mesh does not require a half car model to create useful data, but it will also be useful to see how it behaves with the more complex geometry in the half car model. The wind tunnel size/position test is directly evaluating the half car model, so it is required. The slip floor test also needs the half-car model because the car has many parts in ground effect, and it is important to model these parts for this test. In addition to the listed items, some of the tests originally run in the single element model will be run in the full car model if they appear promising.

Table 4.2: Half-car Simulation Specifications

#	Name	Description
HC1	Baseline	Baseline 2015 half car model
HC2	Cut VC corners	HC1 with excess VC areas removed (see Figure 3.1)
HC3	Polyhedral mesh	HC1 with polyhedral mesh
HC4	PL gap fill %	HC1 with prism layer gap fill percentage altered
HC5	Wind tunnel size/position	HC1 with wind tunnel size and car location adjusted to recommended settings
HC6	Slip floor	HC1 with slip floor

4.3 Simulation Plan

These design changes will be simulated and compared against experimental data using a wind tunnel model and airfoil with published results.

A macro will be used to automatically simulate different angles of attack for any given Star-CCM+ settings. This is very useful because it allows the user to run many simulations without being physically present. This should make it relatively easy to run several hundred simulations over a couple months, instead of several dozen manually. The script also automatically outputs lift and drag data in spreadsheet form, as well as outputting relevant images. These images include the volume mesh, pressure distributions, and velocity profiles, as shown in Figure 4.4. This automated output will make it much easier to analyze the data from many simulations.

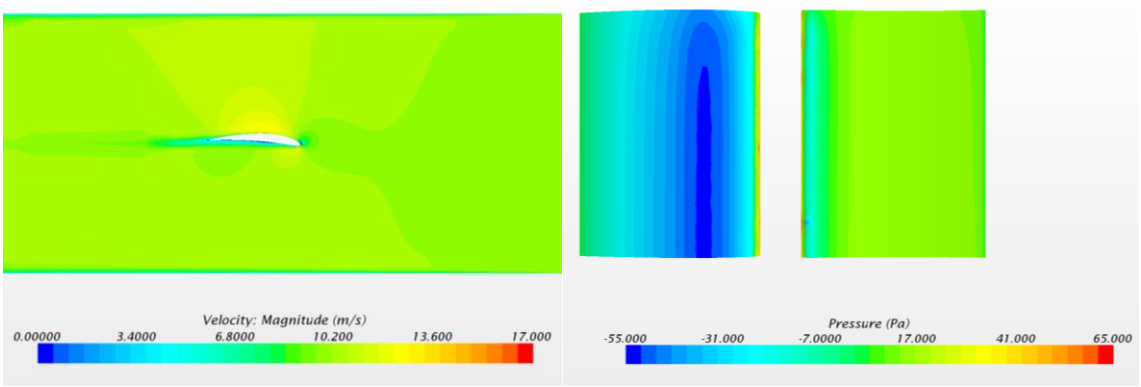

Figure 4.4: Example velocity (left) and pressure profile (right) outputs

It is anticipated that, using the automation features created fall term, it will be reasonable to run and thoroughly analyze one simulation per day. The half-car models will take longer than the single element models, however.

Anticipated Schedule:

- Volumetric controls study (Winter work week)
- Prism layer study (Winter week1)
- k-Omega physics study (Winter week 2)
- Polyhedral mesh study (Winter week 3)
- Per-part settings study (Winter week 4)
- Wind tunnel model study (Winter week 5)
- Yaw study (Winter week 6)
- Pitch/reverse study (Winter week 7)
- Circulation control (blown wing) study (Winter week 8-9)

5. Implementation

5.1 Single Element Wind Tunnel Model

Simulations were run in the single-element wind tunnel model described in section 4. The order of the tests and the parameters tested were changed as noted in Tables 5.1 through 5.4 below. Completed simulations are marked in green; cancelled simulations are marked in red. The macro was updated to output percent difference in mass flow rate in and out of the domain for each angle of attack and provide usability improvements.

Table 5.1 Single-element baseline, volumetric control, and polyhedral mesh simulations

#	Name	Description
BL	Baseline	Standard 2015 settings
VC1	VC scaling 1	BL with VC covering just wing
VC2	VC scaling 2	VC1 with VC scaled 1.5x
VC3	VC scaling 3	VC1 with VC scaled 2x
VC4	VC extension rear	BL with VC scaled 1.5x in x direction; extends rearward
VC5	VC extension front	BL with VC scaled 1.5x in x direction; extends forward
VC6	VC extension top	BL with VC scaled 1.5x in z direction; extend up
VC7	VC extension bottom	BL with VC scaled 1.5x in z-direction; extend down
VC8	Wake refinement	BL with wake refinement turned on
VC9	Surface refinement	BL with no VC; use surface refinement instead
VC10	Wake/surface refinement	VC9 with wake refinement from VC8
VC11	Edge refinement	BL with additional VCs for trailing/leading edge refinement
M1	Polyhedral mesh	BL with polyhedral mesh

The baseline (BL) simulation and the first seven volumetric control (VC) simulations were run as planned. The remaining four VC simulations (VC8-VC11) were decided to be inadequately defined and cancelled. It was decided that more exploration of wake refinement was worthwhile, and a new set of wake refinement (WR) simulations was defined and completed to replace VC8-VC11, as listed in Table 5.2. The polyhedral mesh simulation (M1) was run as planned, but this area was not explored any further.

Table 5.2: Single-element wake refinement simulations

#	Name	Description
WR1	Wake refinement 1	BL with wake refinement added
WR2	Wake refinement 2	WR1 with VCs removed and additional surface refinement
WR3	Wake refinement 3	WR2 with revised wake refinement

WR4	Wake refinement 4	WR3 with more wake refinement and slower growth rate
WR5	Wake refinement 5	WR3 with slower growth rate
WR6	Wake refinement 6	WR3 with prism layer from PR2

All planned prism layer (PL) simulations except PL4 were run, as shown in Table 5.3. PL4 was the same as the baseline and only included by error; it was therefore cancelled. PL1-PL3 were inadvertently run with an incorrect prism layer thickness. The definitions were changed accordingly and PL14-PL16 were added to fit the original definitions of PL1-PL3. PL17-PL25 were added to further explore prism layer behavior with regard to wall y+ value.

Table 5.3: Single-element prism layer simulations

#	Name	Description
PL1	Prism layer 1	BL with 3 prism layers on wing; 7.5mm thickness
PL2	Prism layer 2	BL with 5 prism layers on wing; 7.5mm thickness
PL3	Prism layer 3	BL with 7 prism layers on wing; 7.5mm thickness
PL4	Prism layer 4	BL with 10 prism layers on wing
PL5	Prism layer thickness 1	BL with prism layer thickness 50% smaller
PL6	Prism layer thickness 2	BL with prism layer thickness 50% larger
PL7	Prism layer thickness 3	BL with prism layer thickness 100% larger
PL8	PL convex angle limit	BL with convex angle limit turned on
PL9	PL concave angle limit	BL with concave angle limit turned on
PL10	PL minimum thickness % 1	BL with minimum thickness percentage increased
PL11	PL minimum thickness % 2	BL with minimum thickness percentage decreased
PL12	Layer reduction % 1	BL with layer reduction percentage increased
PL13	Layer reduction % 2	BL with layer reduction percentage decreased
PL14	Prism layer 1	BL with 3 prism layers on wing
PL15	Prism layer 2	BL with 5 prism layers on wing
PL16	Prism layer 3	BL with 7 prism layers on wing
PL17	y+ mesh	Adjust mesh to have theoretically correct wall y+ values large
PL18	y+ mesh	Adjust mesh to have theoretically correct wall y+ values small
PL19	y+ mesh	Adjust WT mesh to have theoretically correct wall y+ values large
PL20	y+ mesh	near wall thickness 2.5 mm
PL21	y+ mesh	near wall thickness 2.0 mm
PL22	y+ mesh	near wall thickness 3.0 mm
PL23	y+ mesh	near wall thickness 0.15 mm
PL24	y+ mesh	near wall thickness 0.10 mm
PL25	y+ mesh	near wall thickness 0.20 mm

The range of physics simulations run was greatly expanded from what was initially planned, and is listed below in Table 5.4. The simulations examined k-omega and k-epsilon turbulence models, and varied the turbulent boundary conditions and initial conditions for each. The varied parameters were turbulent viscosity ratio, length scale, intensity, and velocity scale.

Table 5.4: Single element physics model simulations

#	Name	Description
PH1	k-omega physics model	WR3 with k-omega physics model
PH2	k-omega physics model	PH1 with turb. vel. scale IC = inlet vel.
PH3	k-omega physics model	PH2 with turb. intensity =0.05 for IC and BC
PH4	k-omega physics model	PH3 with more wake refinement
PH5	k-omega physics model	PH3 with viscosity ratio = 5
PH6	k-omega physics model	PH3 with viscosity ratio = 1
PH7	k-omega physics model	PH3 with viscosity ratio = 0.2
PH8	k-omega physics model	PH3 with viscosity ratio = 0.1
PH9	k-omega physics model	begin with k-epsilon solution (WR3); solve w/ k-omega
PH10	k-omega physics model	PH8 with length scale 0.028m
PH11	k-omega physics model	Use length scale 0.014m
PH12	k-omega physics model	Use length scale 0.042m
PH13	k-omega physics model	Use length scale 0.007m
PH14	k-omega physics model	Use length scale 0.100m
PH15	k-omega physics model	Use length scale 0.200m
PH16	k-omega physics model	Use length scale 0.300m
PH17	k-omega physics model	Use length scale 0.400m
PH18	k-omega physics model	Use length scale 0.500m
PH19	k-omega physics model	PH18 with turb.intensity = 0.1000
PH20	k-omega physics model	PH18 with turb.intensity = 0.0100
PH21	k-omega physics model	PH18 with turb.intensity = 0.0050
PH22	k-omega physics model	PH18 with turb.intensity = 0.0010
PH23	k-omega physics model	PH18 with turb.intensity = 0.0005
PH24	k-epsilon physics model	ti=0.1; ls=0.5
PH25	k-epsilon physics model	ti=0.1; ls=0.4
PH26	k-epsilon physics model	ti=0.1; ls=0.3
PH27	k-epsilon physics model	ti=0.1; ls=0.2
PH28	k-epsilon physics model	ti=0.1; ls=0.1
PH29	k-epsilon physics model	ti=0.08; ls=0.5

PH30	k-epsilon physics model	ti=0.06; ls=0.5
PH31	k-epsilon physics model	ti=0.04; ls=0.5
PH32	k-epsilon physics model	ti=0.02; ls=0.5
PH33	k-epsilon physics model	ti=0.01; ls=0.5

5.1.0 Baseline

A new baseline was developed for the GFR 2015 half-car model based on the 2014 model. The biggest change was to the prism layers: instead of two prism layers with a total thickness of 100mm, the 2015 model used 10 prism layers with a total thickness of 5mm (on wings) or 10mm (on other car parts). Volumetric controls were moved to match the new wing locations. This new model improved some aspects of the prism layer, such as abrupt cut-offs and missing prism layers shown in Figure 5.1. These problems are not present in the 2015 model, shown in Figure 5.2. However, the 2015 mesh still has issues, such as a jagged leading edge. We also did not have evidence to demonstrate what prism layer thickness was appropriate. To further develop this mesh, a single-element wing wind tunnel mesh was created using the same parameters as the 2015 half-car baseline. This model was designated "baseline" (BL) and was the starting point for further development in the single-element wind tunnel model.

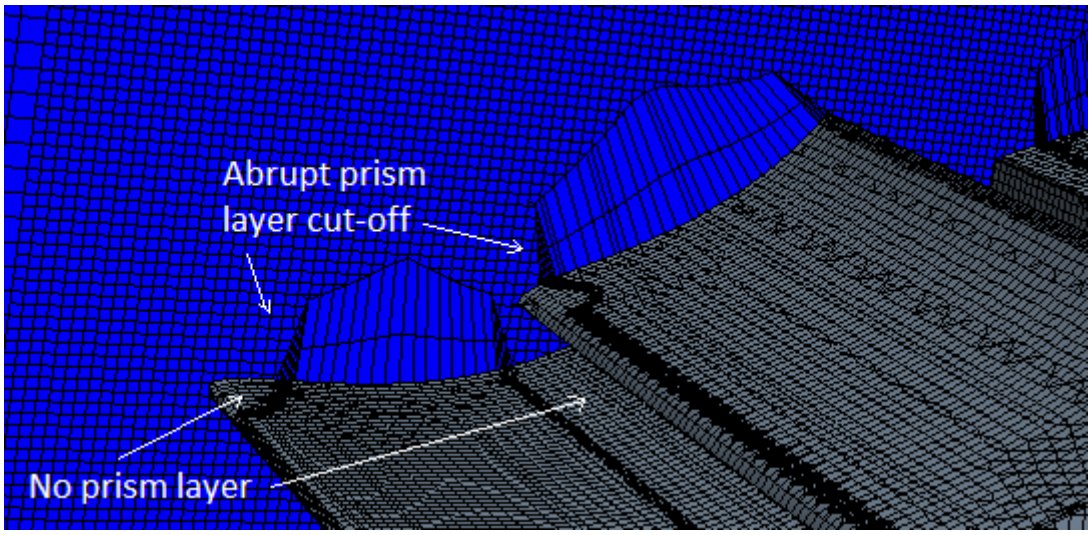

Figure 5.1: 2014 Half-car model mesh showing front wing (grey) and symmetry plane (blue)

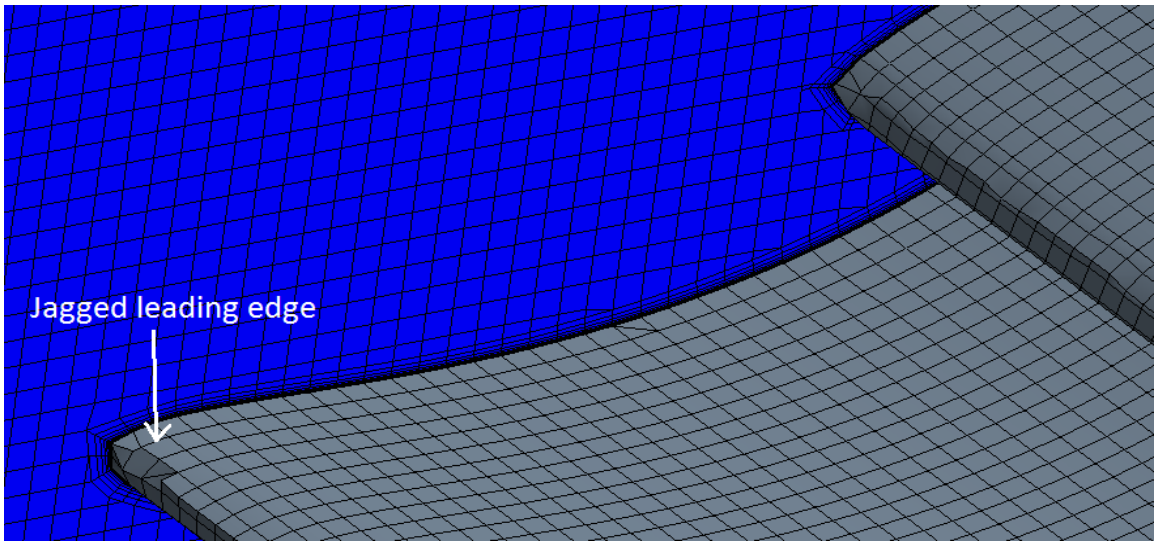

Figure 5.2: 2015 Half-car model showing rear wing (grey) and symmetry plane (blue)

The baseline (BL) single-element wind tunnel simulation was created using the geometry discussed in section 4.2 and the mesh and physics parameters from the 2015 half-car simulation. A selection of important values are listed below in Table 5.5.

Table 5.5: Baseline (BL) single-element simulation parameters

Mesh	
Base size	1 m
Prism layer thickness (global)	10 mm
Number of prism layers (global)	5
Prism layer stretching (global)	1.5
Car VC customizations	Prism layer mesher, surface remesher, surface wrapper, trimmer isotropic size
Mesh absolute size (car VC)	30 mm
Prism layer thickness (car VC)	10 mm
Number of prism layers (car VC)	8
Prism layer stretching (car VC)	1.5
Wing VC customizations	Prism layer mesher, surface remesher, surface wrapper, trimmer isotropic size
Mesh absolute size (wing VC)	10 mm
Prism layer thickness (wing VC)	5 mm
Number of prism layers (wing VC)	10
Prism layer stretching (wing VC)	1.5
Physics	
Models	Steady

	Three dimensional
	Turbulent
	Constant density
Turbulence Models	Reynolds Averaged Navier Stokes
	K-Epsilon Realizable Two-Layer
Wall treatment	Two-layer all y+
Flow Solver	Segregated Flow
Initial Conditions	
Turbulence Intensity	0.01
Turbulent Velocity Scale	1 m/s
Turbulent Viscosity Ratio	10
Velocity	[-22.1564, 0, 0] mph
Boundary Conditions	
Symmetry plane	symmetry
Inlet boundary type	velocity inlet
Inlet Turbulence Intensity	0.01
Inlet Turbulent Viscosity Ratio	10
Inlet Velocity Magnitude	22.1564 mph
Outlet boundary type	Pressure outlet
Outlet Turbulence Intensity	0.01
Outlet Turbulent Viscosity Ratio	10
Outlet pressure	0.0 Pa gage

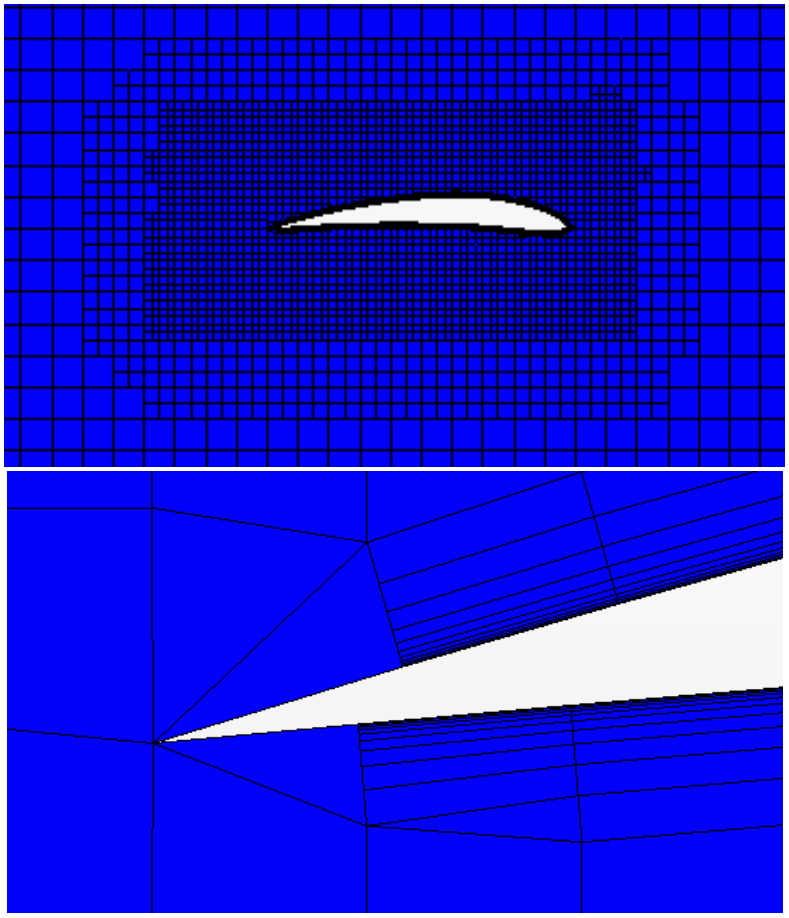

Figure 5.3: Baseline (BL) mesh around wing (top) and trailing edge detail view (bottom)

Lift and drag coefficient are calculated in CFD for each angle of attack and output in a .csv file. These values are shown for reference in Table 5.6 and plotted compared to wind tunnel data in Figures 5.3 and 5.4. Using the difference between CFD results and wind tunnel data at each angle of attack, a mean approximate error is calculated to quantify the total difference between wind tunnel and CFD results. This value is calculated as:

$$MAE_{Cf} = \sqrt{\sum_{i} \left(Cf_{WT_i} - Cf_{CFD_i}\right)^2}$$

where MAE is mean approximate error, Cf is a force coefficient (either Cl or Cd), i is angle of attack, and WT and CFD refer to the wind tunnel and CFD results respectively. These values are also reported in Table 5.6.

Table 5.6: Baseline (BL) CFD Lift and Drag coefficients and corresponding wind tunnel data

	CFD		Wind Tunnel	
AoA	Cl	Cd	Cl	Cd
-2.89	0.317	0.036	0.285	0.0193

-1.38	0.506	0.0275	0.437	0.015
0.21	0.718	0.0265	0.602	0.0145
1.66	0.857	0.0276	0.744	0.0135
3.32	1.024	0.0334	0.903	0.0147
4.95	1.171	0.0421	1.059	0.0157
6.94	1.228	0.0584	1.238	0.0179
8.08	1.224	0.0716	1.328	0.0197
10.1	1.212	0.0968	1.426	0.0239
11.3	1.284	0.1088	1.406	0.0314
MAE	0.121	0.044		

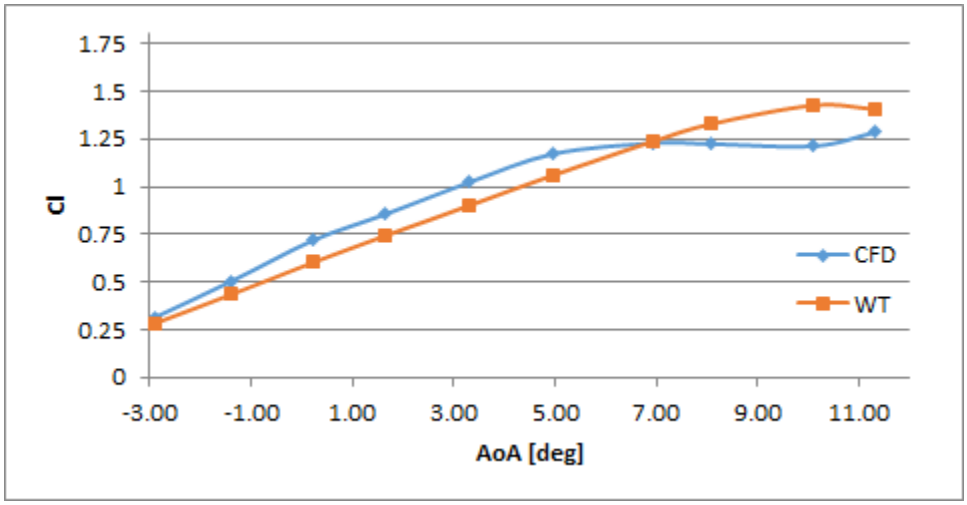

Figure 5.4: Baseline (BL) CFD lift coefficient vs AoA compared to wind tunnel (WT) data

As shown in Figure 5.4, CFD results for Cl follow the same general trend as wind tunnel results for AoA less than 7°, but are higher. Around 7°, CFD results flatten out and decrease up until 10°. Wind tunnel data continue to increase up until 10°, and then decrease at 11°. CFD results increase at 11°, but are still lower than wind tunnel data. This early decline suggests that stall and flow separation are occurring at a lower angle of attack in CFD than they did in the wind tunnel. This theory is supported by the velocity visualizations in Figure 5.5. There is a low velocity (blue) section on the upper side of the trailing edge of the 1.6° AoA wing, but there is no visible recirculation, at least at the mesh resolution used. A small amount of recirculation is visible at 3.32° AoA. The size of the recirculation/separation zone increases moderately at 4.95° and 6.94° AoA, and then increases dramatically at 8.08° AoA and beyond. This mimics the decrease in lift seen in the simulation. The cause of the increase at 11.30° is uncertain. It is possible that the separation is so significant at this point that the flow is transient and cannot be realistically modelled in a steady state simulation.

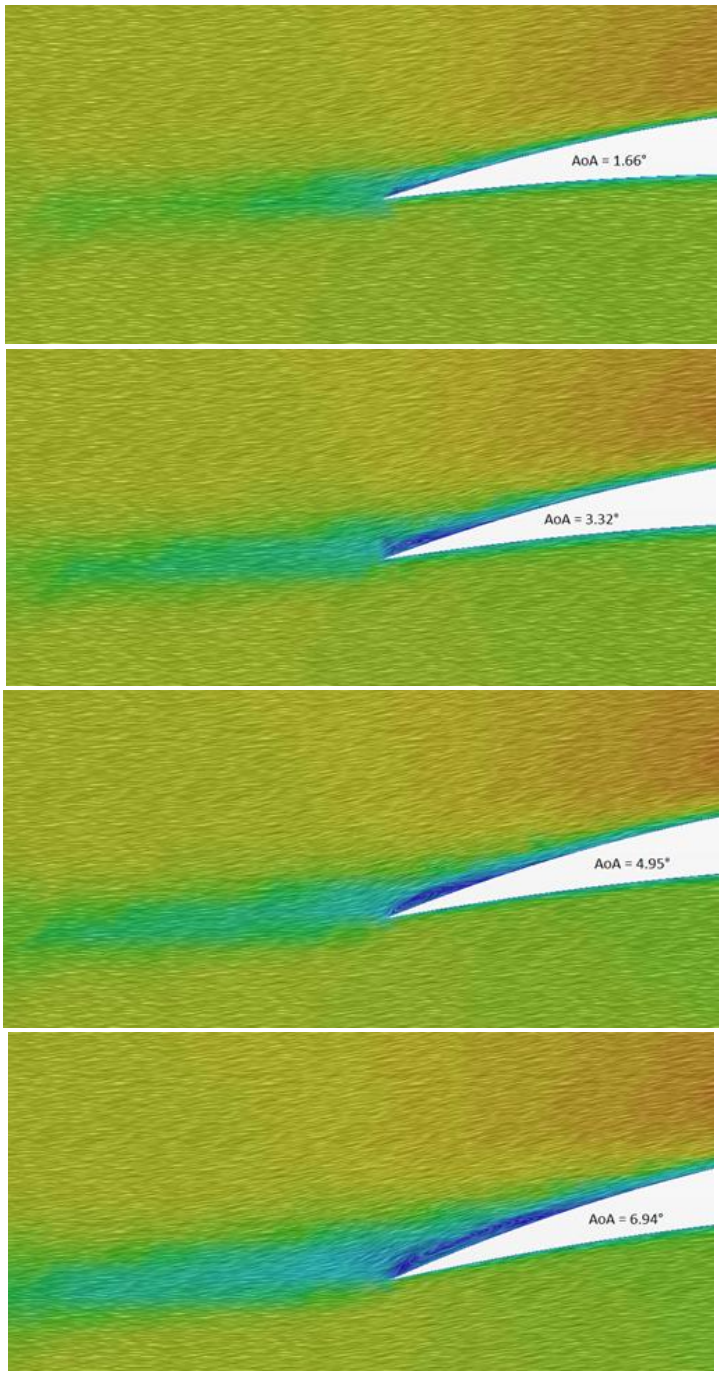
AoA = 1.66°
AoA = 3.32°
AoA = 4.95°
AoA = 6.94°

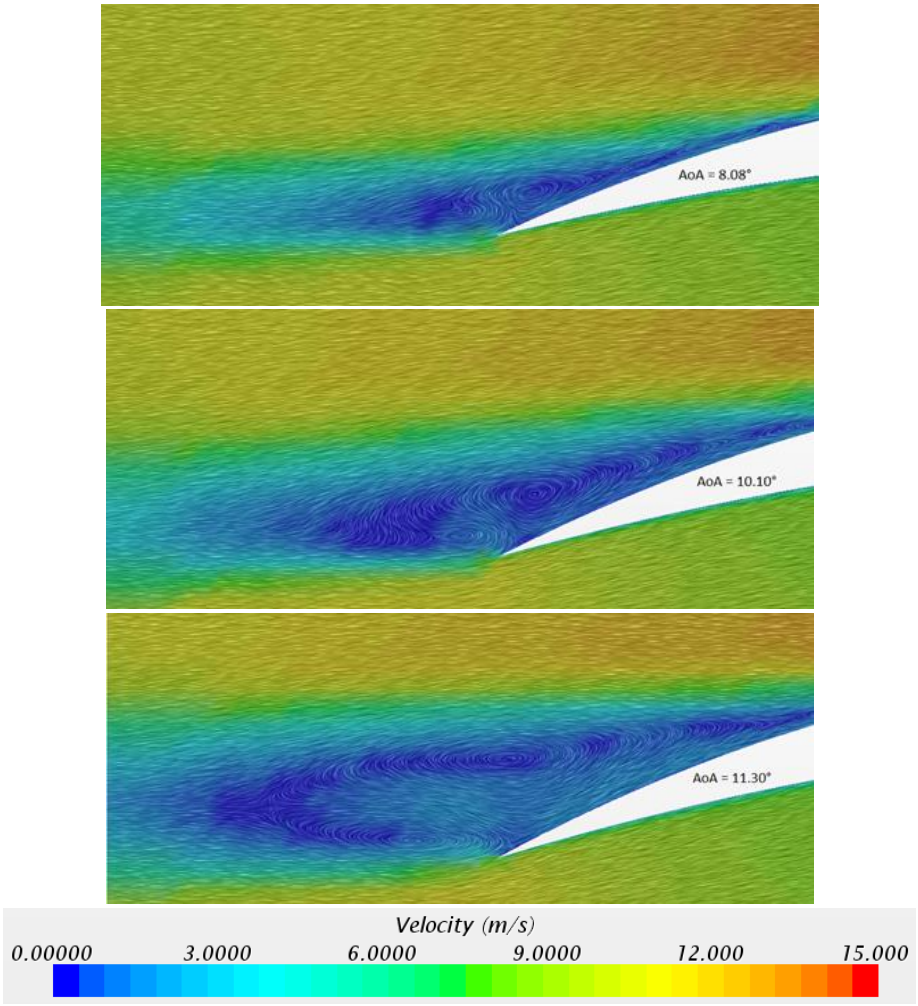

Figure 5.5: Trailing edge flow separation visualized with velocity line integral convolution for baseline (BL) at different angles of attack, on the symmetry plane.

Drag coefficient values for the BL simulation are plotted with the wind tunnel results in Figure 5.6. The CFD results are significantly higher than the wind tunnel results at all angles of attack. CFD drag coefficients are approximately twice as large as wind tunnel results at low angles of attack, and increase to more than three times as large at high angles of attack. This increased discrepancy at high angle of attack correlates with the increase in flow separation at these angles. If the increase in flow separation in CFD is not realistic, this would cause an artificial increase in drag, which matches what was seen in the CFD results. The cause of the discrepancy at low angles of attack is not known. This will be explored further in more simulations.

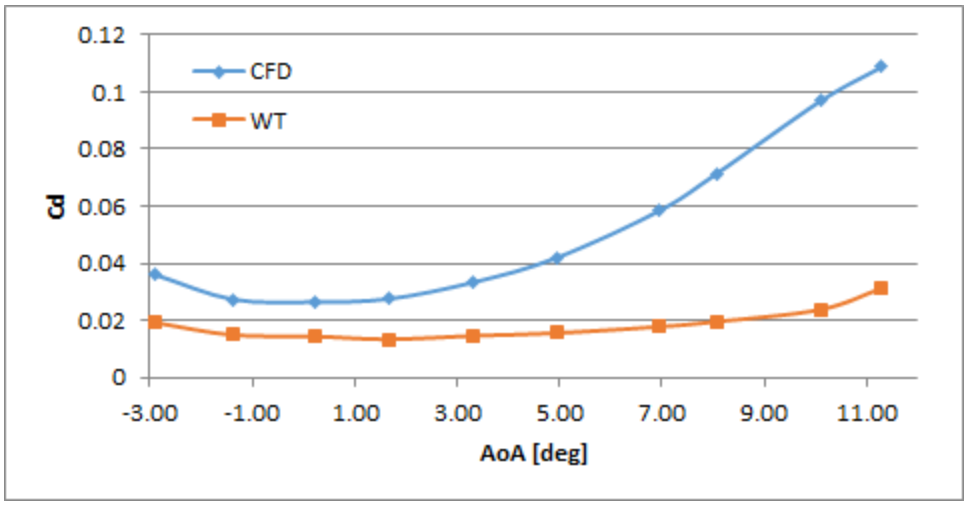

Figure 5.6: Baseline (BL) CFD drag coefficient vs AoA compared to wind tunnel (WT) data

5.1.1 Prism Layers

The prism layer (PL) simulations took the baseline mesh and altered the prism layer parameters, attempting to better simulate the boundary layer region of the wing. This region was studied intensively because flow separation begins in the boundary layer, and it is important to GFR to model this accurately. These simulations fall into two distinct groups: Simulations assessing sensitivity of the baseline model to changes in prism layer parameters, and simulations attempting to model the boundary layer correctly by designing the mesh to have a particular wall y+ value. Parameter sensitivity is discussed first.

Simulations PL1-3, 5-7, and 14-16 altered the parameters "prism layer thickness" and "number of prism layers" around the wing. The prism layer thickness measures the combined thickness of all layers in the prism layer, measured normal to the part surface. These values were set using a volumetric control. The values for each simulation are listed below in Table 5.7.

Table 5.7: Prism layer (PL) 1-3, 5-7, and 14-16 single element simulation parameters

Simulation	Parameter	Value
BL	Prism layer thickness	5 mm
	Number of prism layers	10
PL1	Prism layer thickness	7.5 mm
	Number of prism layers	3
PL2	Prism layer thickness	7.5 mm
	Number of prism layers	5
PL3	Prism layer thickness	7.5 mm
	Number of prism layers	7
PL5	Prism layer thickness	2.5 mm

	Number of prism layers	10
PL6	Prism layer thickness	7.5 mm
	Number of prism layers	10
PL7	Prism layer thickness	10 mm
	Number of prism layers	10
PL14	Prism layer thickness	5 mm
	Number of prism layers	3
PL15	Prism layer thickness	5 mm
	Number of prism layers	5
PL16	Prism layer thickness	5 mm
	Number of prism layers	7

These values were selected to provide a range near the baseline. No number of prism layers greater than 10 was selected because this baseline value was already well above the CD-adapco recommended values. Instead, a wider range of smaller values was explored. The lift coefficient MAE and drag coefficient MAE for these simulations are plotted below in Figure 5.7 and Figure 5.8. The best result for lift coefficient was with 5 prism layers and 7.5 mm thickness (PL2). Drag coefficient also had the lowest error in PL2, although it also had a similarly small error with 3 prism layers and 5 mm thickness (PL14). PL2 is selected as the best result because it had low error for both lift and drag. It is theorized that thinner prism layers are less accurate because they are not large enough to model the entire boundary layer. Thicker boundary layers were not thoroughly explored, and could be a subject for future simulations. Similarly, it is believed that having too few prism layers did not provide enough resolution to accurately model the boundary layer. It is less clear why having more prism layers would reduce accuracy. It is possible that adding more prism layers puts the wall y+ value in the buffer layer, which was found by Salim and Cheah to reduce accuracy [12], as discussed in Section 2. This may explain the increase and then decrease in error for both lift and drag as the number of prism layers increased from 5 (PL2) to 7 (PL3) to 10 (PL6) at thickness 7.5 mm. The highest error would be with wall y+ values in the buffer layer, and lower error with wall y+ values in the viscous sublayer and log-law region. This is not completely supported by the wall y+ values output by Star-CCM+, shown in Figure 5.9. Using the definitions from Salim and Cheah, PL1 was mostly in the log-law region ($y+>30$) and PL6 was mostly in the viscous sublayer ($y+<5$), but PL2 and PL3 both had a large portion of their surfaces in the buffer layer ($5<y+<30$). It is possible that PL2 y+ values were close enough to the log-law region that they were able to be resolved accurately, or that Salim and Cheah's results are not applicable to this situation.

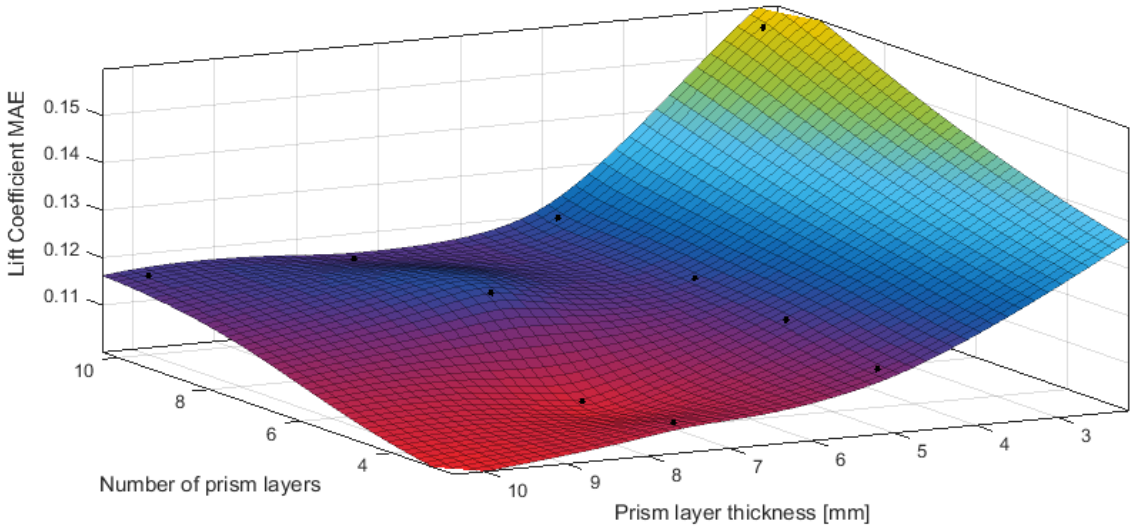

Figure 5.7: Lift coefficient MAE for prism layer simulations, plotted vs. prism layer thickness and number of prism layers

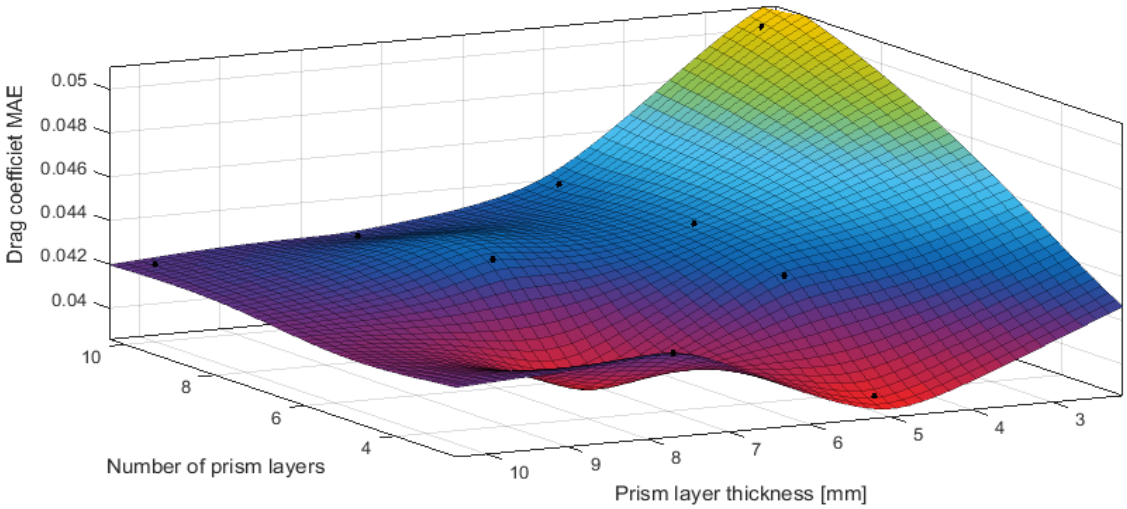

Figure 5.8: Drag coefficient MAE for prism layer simulations, plotted vs. prism layer thickness and number of prism layers

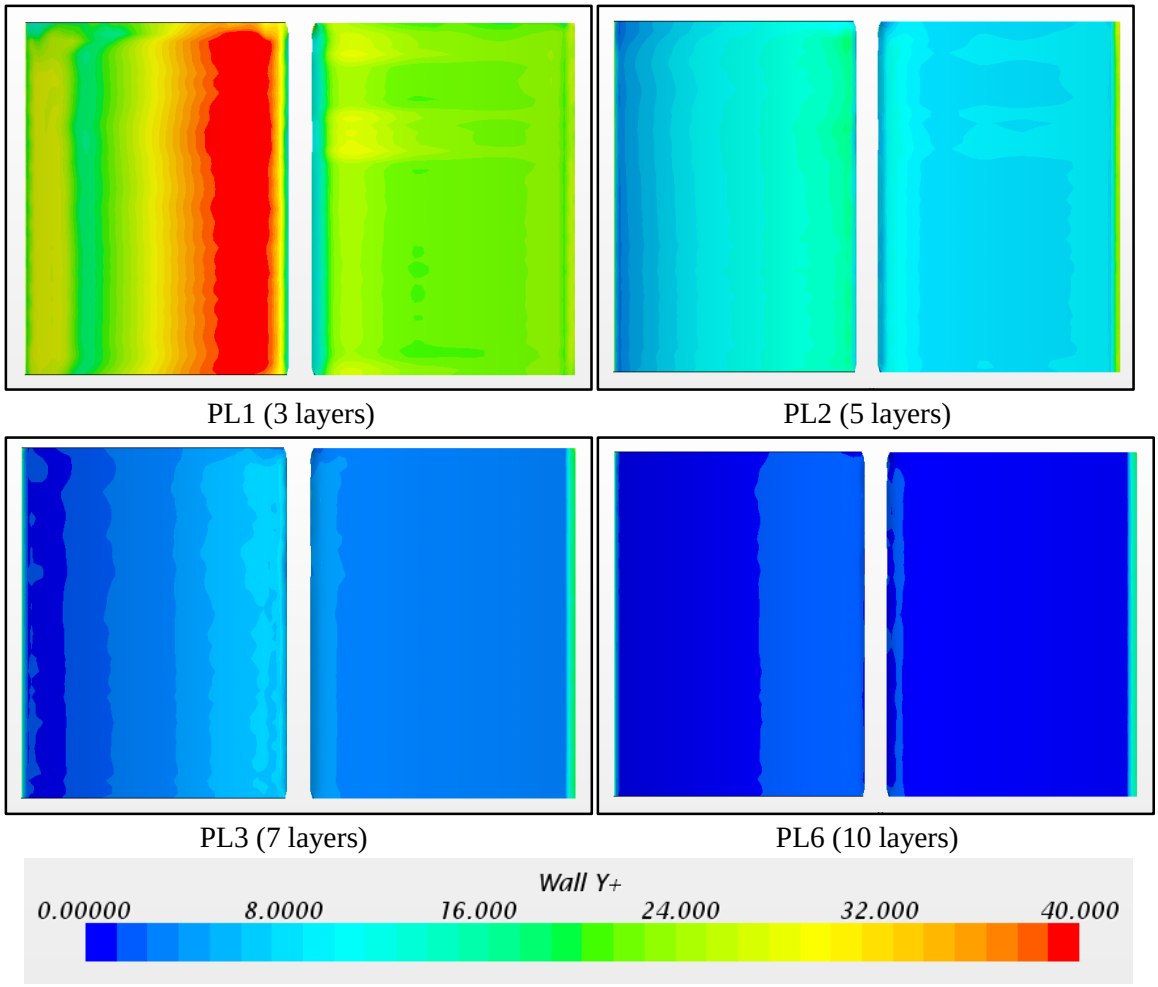

Figure 5.9: Wall y+ values for PL simulations with 7.5 mm prism layer thickness, at 4.96º AoA. Top wing surface shown on the left; bottom surface on the right.

Simulations PL8-PL13 looked at the effect of altering other parameters related to the prism layer tool, with the goal of producing a smoother or more uniform prism layer. These parameters include convex angle limit, concave angle limit, prism layer minimum thickness percentage, and layer reduction percentage. The definitions and effects of these parameters are discussed in Section 3.3. The altered parameters for each simulation are shown below in Table 5.8.

Table 5.8: Prism layer (PL) 8-13 single element simulation parameters

Simulation	Parameter	Value
BL	convex angle limit	off (360º)
	concave angle limit	off (0º)
	minimum thickness %	10%
	layer reduction %	50%

PL8	convex angle limit	320º
PL9	concave angle limit	95º
PL10	minimum thickness %	30%
PL11	minimum thickness %	5%
PL12	layer reduction %	75%
PL13	layer reduction %	25%

The MAE for the lift and drag coefficients in these simulations are plotted below in Figure 5.10. None of these parameter changes resulted in large differences in error compared to baseline, but some helped slightly. Adding a convex angle limit in PL8 made only a very small improvement to lift coefficient accuracy, and reduced drag coefficient accuracy. The concave angle limit in PL9 slightly improved accuracy for both drag coefficient and lift coefficient. Increasing the minimum thickness percentage in PL10 made a larger improvement to lift coefficient accuracy, and a small improvement to drag coefficient accuracy. Decreasing the minimum thickness percentage in PL11 had the opposite effect, reducing accuracy. Increasing the layer reduction percentage in PL13 slightly increased lift coefficient accuracy while reducing drag coefficient accuracy. Decreasing the layer thickness percentage in PL14 reduced lift coefficient accuracy and increased drag coefficient accuracy.

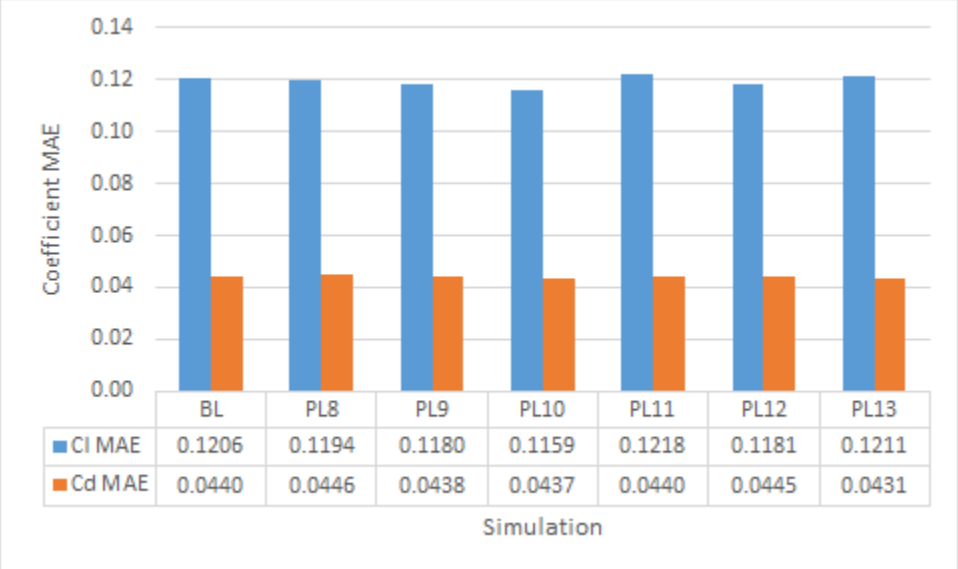

Figure 5.10: MAE for lift and drag coefficients in simulations PL8-PL13

Based on these results, it is recommended that a concave angle limit be used and the minimum thickness percentage be increased from baseline. These both provided positive changes to both lift and drag coefficient accuracy. A sensitivity study could be performed to find the best values for each of these parameters. Convex angle limit and layer reduction percentage both had inconclusive results--changing the parameter to increase lift accuracy decreased drag accuracy. It

is therefore not recommended to change these two parameters from baseline without more information.

Simulations PL17-PL29 altered the prism layer with the goal of achieving wall y+ values as recommended by Salim and Cheah [12]. This set of simulations used a different simulation--PH19--as a baseline. PH19 was developed based on the earlier prism layer studies (PL1-PL16), improved wake refinement (mesh from WR3) and a different physics model, which was found to be more accurate (k-omega). Wake refinement and physics development are discussed in section 5.1.3 and 5.1.4 below. After developing those areas, the best simulation (PH19) was used as a baseline for further prism layer development, which is described here. For these simulations, prism layer properties were specified for individual parts (boundaries) instead of using volumetric controls. The properties for these simulations are listed below in Table 5.9.

Table 5.9: Prism layer (PL) 17-25 single element simulation parameters

Simulation	Parameter	Value
PH19	Prism layer thickness (global)	10 mm
	Number of prism layers (global)	5
	Prism layer stretching (global)	1.5
	Layer reduction percentage	50
	Prism layer thickness (wing)	15 mm
	Number of prism layers (wing)	4
	Wall treatment	all wall y+
PL17	Layer reduction percentage	100
PL18	Number of prism layers (wing)	10
PL19	Prism layer thickness (global)	20 mm
	Number of prism layers (global)	4
	Layer reduction percentage	100
PL20	Near wall thickness (global)	2.5 mm
	Prism layer thickness (global)	20 mm
	Number of prism layers (global)	4
	Prism layer thickness (wing)	use global
	Number of prism layers (wing)	use global
PL21	Near wall thickness (global)	2.0 mm

	Other settings same as PL20	
PL22	Near wall thickness (global)	3.0 mm
	Other settings same as PL20	
PL23	Near wall thickness (global)	0.15 mm
	Other settings same as PL20	
PL24	Near wall thickness (global)	0.10 mm
	Other settings same as PL20	
PL25	Near wall thickness (global)	0.20 mm
	Other settings same as PL20	

PL17 attempts to keep wall y+ values for the wing in the log-law region, with 30<y+<60. It keeps the same prism layer thickness and number of prism layers as the baseline PH19, but changes the layer reduction percentage to avoid small near wall cells near the leading and trailing edges where the prism layer begins to shrink. This effect is illustrated in Figure 5.11. Note that the leading edge in PH19 has four prism layers and is thinner than the prism layer away from the leading edge. Therefore, the near wall cell is thinner, and has a lower wall y+ value than other parts of the wing. In PL17, the prism layer reduces the number of layers to three when it becomes thinner near the leading edge. This allows the near wall cell to remain thicker, and maintain a wall y+ value similar to the rest of the wing. This change produced a significant improvement to lift coefficient accuracy, but actually decreased drag coefficient accuracy. These results are shown in Figure 5.12.

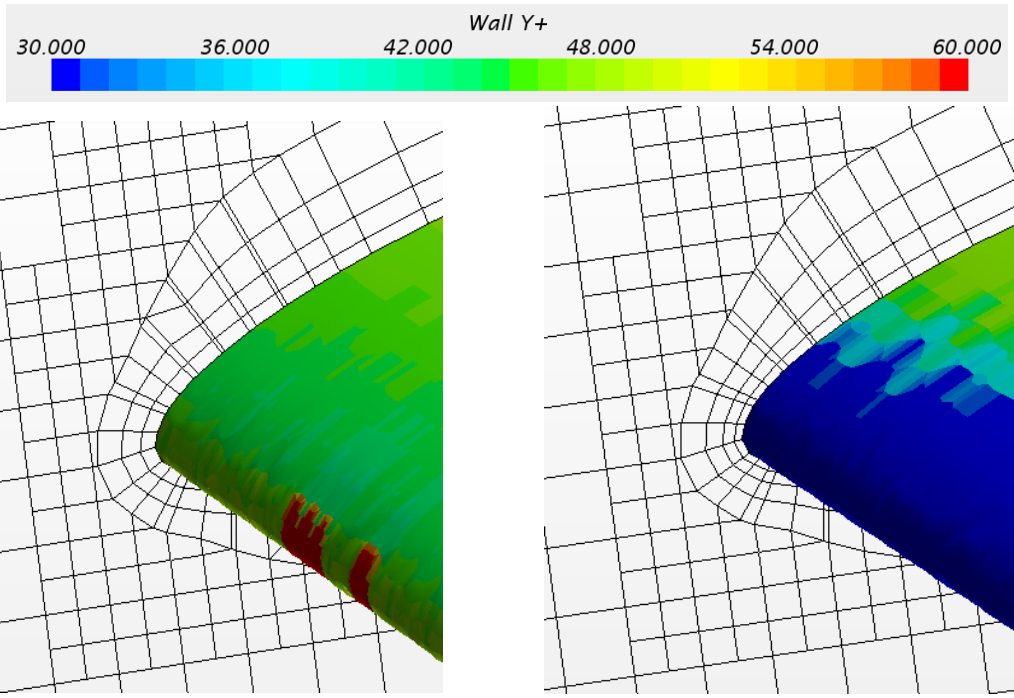

PL17 PH19

Figure 5.11: Mesh and wall y+ values near the leading edge for PL17 and PH19 at AoA 0.21º

PL18 reduced the wall y+ values to the viscous sublayer range (y+<5) around the wing by adding additional prism layers and keeping the same prism layer thickness. It did not change layer reduction percentage from PL19 because there is not a lower bound on wall y+ values for this range, so it is acceptable to have smaller wall y+ values near the leading and trailing edges. This reduced lift coefficient accuracy compared to PH19, and very slightly increased drag coefficient accuracy.

PL19 kept the settings around the wing the same, but tried to apply the same wall y+ conditions to the entire wind tunnel by changing the global the prism layer thickness and number of prism layers. This generated wall y+ values in the log-law range for the endplate and wind tunnel walls. Surprisingly, this significantly reduced accuracy for both the lift and drag coefficients.

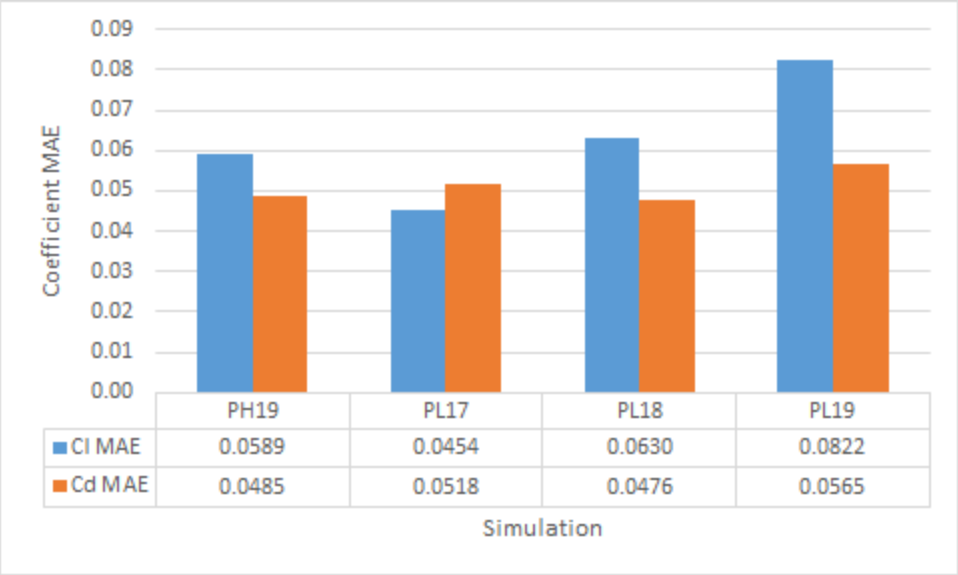

Figure 5.12: MAE for lift and drag coefficients in simulations PL17-PL19

PL20-PL25 used a different method to alter the wall y+ value. Instead of using the "prism layer stretching" parameter to define thickness of individual prism layers, these simulations used the "near wall thickness" parameter, which allow the user to directly specify the thickness of near-wall cells. This is useful because it makes it easier to change the near-wall thickness without having to back-calculate it based on the prism layer stretching parameter, and allows it to remain constant even when the prism layer shrinks. It still does not allow the user to specify a uniform wall y+ value, however, because wall y+ is dependent on a reference velocity, which varies at different locations along the wing. PL20-PL22 tried values in the log-law region, and PL23-PL26 tried values in the viscous sublayer region. None of these results performed as well as PL19. Lift coefficient error was consistently higher, and drag coefficient error was higher in all but one case. In the viscous sublayer region simulation, lift coefficient error rapidly increased as near wall thickness decreased.

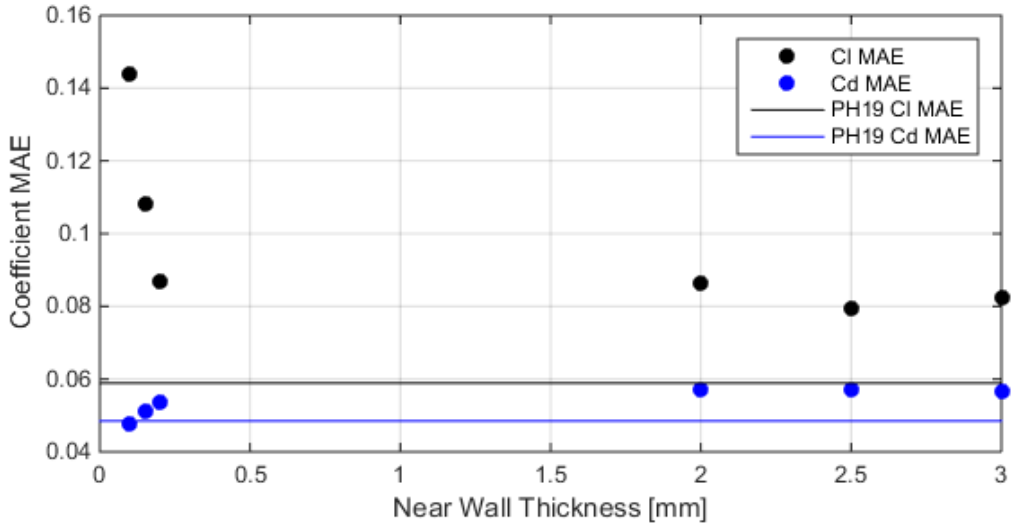

Figure 5.13: Lift and drag coefficient MAE plotted vs near wall thickness for PL20-25, with results from PH19 shown as lines for comparison.

Using the near wall thickness parameter did not create any better results, but because it is very easy to use, it probably deserves further simulation to see if it can be used accurately. Exploring different wall y+ values or different prism layer thicknesses and numbers of prism layers could yield better results.

5.1.2 Volumetric Controls

The volumetric control (VC) simulations again started with the baseline (BL) simulation. This time, changes were made to the size and location of the volumetric control around the wing. The location of the volumetric control determines which areas of the mesh are most refined, which lets it more accurately solve higher gradients in simulated variables. The size of the volumetric control is a trade-off between accuracy and cell count. High accuracy is desired, but a high cell count slows down the simulation. The parameters for simulations VC1-VC7 are listed below in Table 5.10.

Table 5.10: Volumetric Control (VC) 1-7 single element simulation parameters

Simulation	Parameter	Value
BL	VC corners	[-1.325, 0.0, 0.320] [-0.850, 0.532, 0.550] [m]
VC1	VC corners	[-1.225, 0.0, 0.384] [-0.905, 0.437, 0.462] [m]
VC2	VC corners	[-1.097, 0.0, 0.366] [-1.303, 0.437, 0.483] [m]
VC3	VC corners	[-0.741, 0.0, 0.348] [-1.381, 0.437, 0.504] [m]
VC4	VC corners	[-0.850, 0.0, 0.319] [-1.563, 0.531, 0.550] [m]
VC5	VC corners	[-0.612, 0.0, 0.319] [-1.325, 0.531, 0.550] [m]
VC6	VC corners	[-0.850, 0.0, 0.319] [-1.325, 0.531, 0.665] [m]
VC7	VC corners	[-0.850, 0.0, 0.204] [-1.325, 0.531, 0.550] [m]

The baseline (BL) simulation had an arbitrarily placed volumetric control (VC) which covered the wing and a small amount of the surrounding area, as shown below in Figure 5.14. It was designed to refine the mesh on the wing surface and the area nearest the wing. In each simulation run here, the wing VC covers the entire width of the wing, from the symmetry plane to the endplate. Results are shown in Figure 5.15. VC1 reduced the size of the volumetric control to cover only the wing, at all angles of attack. Unexpectedly, this reduced error in lift coefficient, but it did increase error in drag coefficient. VC2 uniformly scaled up the volumetric control from VC1 by a factor of 1.5. This resulted in the lowest error of any of the VC simulations. VC3 uniformly scaled up the volumetric control from VC1 by a factor of 2. VC4-VC7 used BL as a starting point, and each extended the volumetric control in a different direction: backwards (-x), forwards (+x), up (+z) and down (-z), respectively. None of these four changes had a large impact on accuracy, and extending the volumetric control forward in VC5 actually reduced it.

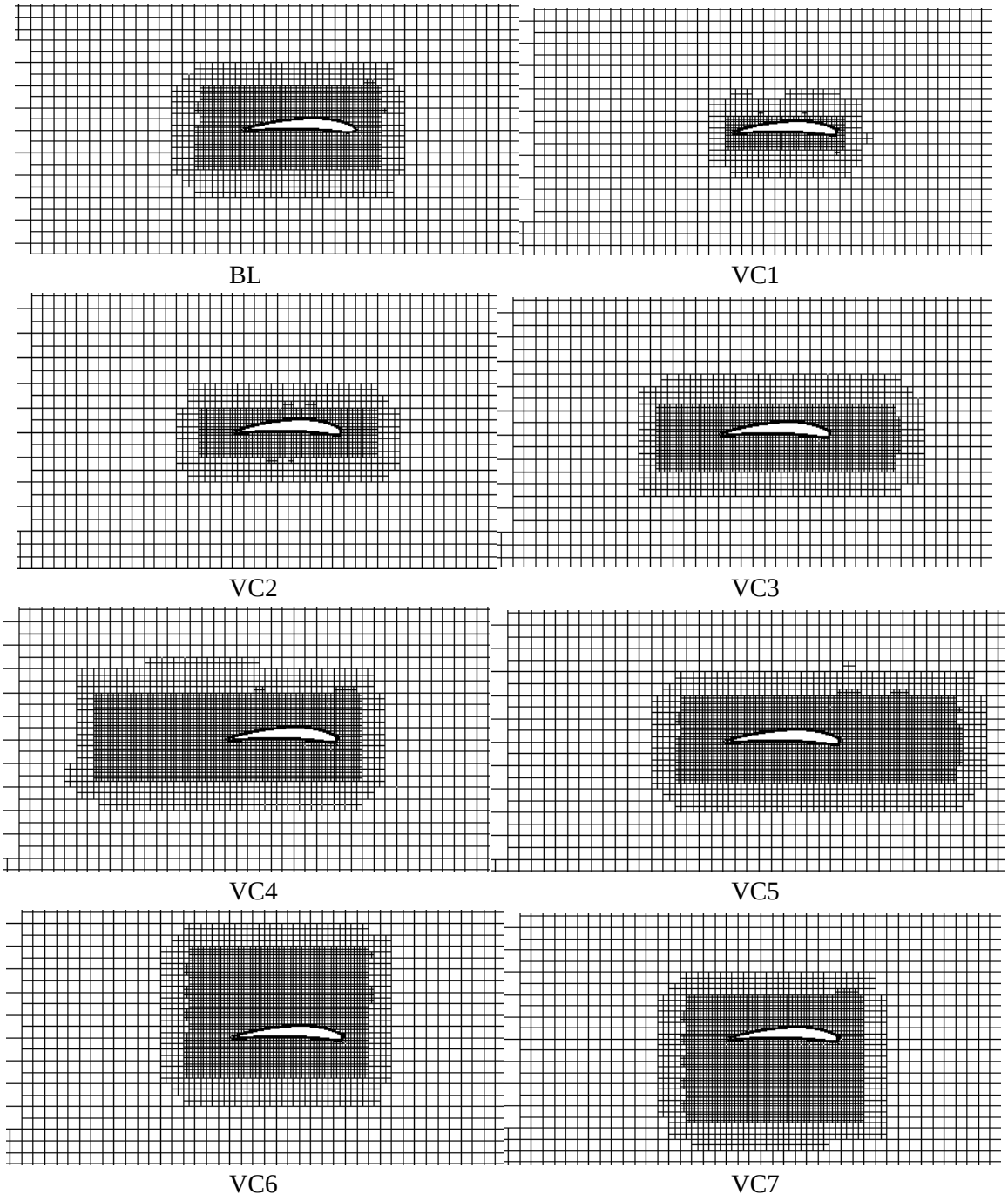

Figure 5.14: Symmetry plane meshes for BL and VC1-VC7, illustrating the location of the wing volumetric control at AoA=0.21º

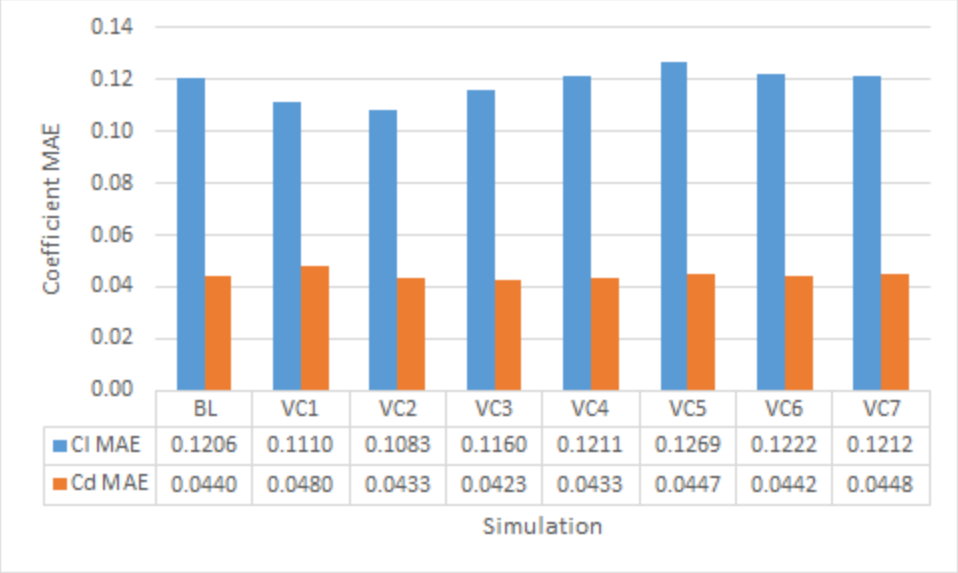

Figure 5.15: MAE for lift and drag coefficients in simulations VC1-VC7

Based on these results, it was decided that, without referencing the solution, changing the size and location of the volumetric control did not predictably improve results. A new set of simulations, titled Wake Refinement (WR), was created to more methodically and iteratively determine the best way to refine the mesh.

5.1.3 Wake Refinement

The wake refinement (WR) simulations use the wake refinement tool in Star-CCM+ to refine the mesh around the wing, and refine boundary surfaces on a per-part basis. BL is used as a baseline. Parameters for each simulation are listed below in Table 5.11.

Table 5.11: Wake refinement (WR) 1-6 single element simulation parameters

Simulation	Parameter	Value	
BL	Wake refinement	none	
	Volumetric controls	wing, "car" (wing and endplate area)	
	Default growth rate	Medium	
WR1	Wake refinement	Boundaries	NACA-6409 (wing)
		Distance	1.2 m [-1, 0, 0]
		Cell size	15 mm
WR2	Volumetric controls	none	
	NACA-6409 mesh values	Number of prism layers	4

		Prism layer thickness	15 mm
		Surface size	10 mm target; 2 mm minimum
		Boundary growth layers	2
	Wake refinement	Boundaries	NACA-6409 (wing)
		Distance	1.5 m [-1, 0, 0]
		Cell size	10 mm
WR3	Volumetric controls		none
	NACA-6409 mesh values	Number of prism layers	4
		Prism layer thickness	15 mm
		Surface size	10 mm target; 2 mm minimum
		Boundary growth layers	2
	Far Wake refinement	Boundaries	NACA-6409 (wing)
		Distance	0.7 m [-1, 0, 0]
		Cell size	20 mm
	Near Wake refinement	Boundaries	NACA-6409 (wing)
		Distance	0.3 m [-1, 0, 0]
		Cell size	10 mm
	Upper Wake refinement	Boundaries	NACA-6409 (wing)
		Distance	0.3 m [0, 0, 1]
		Cell size	20 mm
WR4	Volumetric controls		none
	NACA-6409 mesh values	Number of prism layers	4
		Prism layer thickness	15 mm
		Surface size	10 mm target; 2 mm minimum
		Boundary growth layers	2
	Far Wake refinement	Boundaries	NACA-6409 (wing)
		Distance	0.7 m [-1, 0, 0]

		Cell size	20 mm
	Near Wake refinement	Boundaries	NACA-6409 (wing)
		Distance	0.3 m [-1, 0, 0]
		Cell size	10 mm
	Upper Wake refinement	Boundaries	NACA-6409 (wing)
		Distance	0.3 m [0, 0, 1]
		Cell size	20 mm
	Lower Wake refinement	Boundaries	NACA-6409 (wing)
		Distance	0.1 m [0, 0, -1]
		Cell size	20 mm
	Default growth rate		Slow
WR5	Volumetric controls		none
	NACA-6409 mesh values	Number of prism layers	4
		Prism layer thickness	15 mm
		Surface size	10 mm target; 2 mm minimum
		Boundary growth layers	2
	Far Wake refinement	Boundaries	NACA-6409 (wing)
		Distance	0.7 m [-1, 0, 0]
		Cell size	20 mm
	Near Wake refinement	Boundaries	NACA-6409 (wing)
		Distance	0.3 m [-1, 0, 0]
		Cell size	10 mm
	Upper Wake refinement	Boundaries	NACA-6409 (wing)
		Distance	0.3 m [0, 0, 1]
		Cell size	20 mm
	Default growth rate		Slow
WR6	Volumetric controls		none

	NACA-6409 mesh values	Number of prism layers	5
		Prism layer thickness	7.5 mm
		Surface size	10 mm target; 2 mm minimum
		Boundary growth layers	2
	Far Wake refinement	Boundaries	NACA-6409 (wing)
		Distance	0.7 m [-1, 0, 0]
		Cell size	20 mm
	Near Wake refinement	Boundaries	NACA-6409 (wing)
		Distance	0.3 m [-1, 0, 0]
		Cell size	10 mm
	Upper Wake refinement	Boundaries	NACA-6409 (wing)
		Distance	0.3 m [0, 0, 1]
		Cell size	20 mm

WR1 added refinement in the wake behind the wing, using the wake refinement tool. It used the same volumetric controls as the baseline and did not change any per-part settings. The refined wake is shown below in Figure 5.15. This had very little impact on the accuracy of the result, as shown in Figure 5.16.

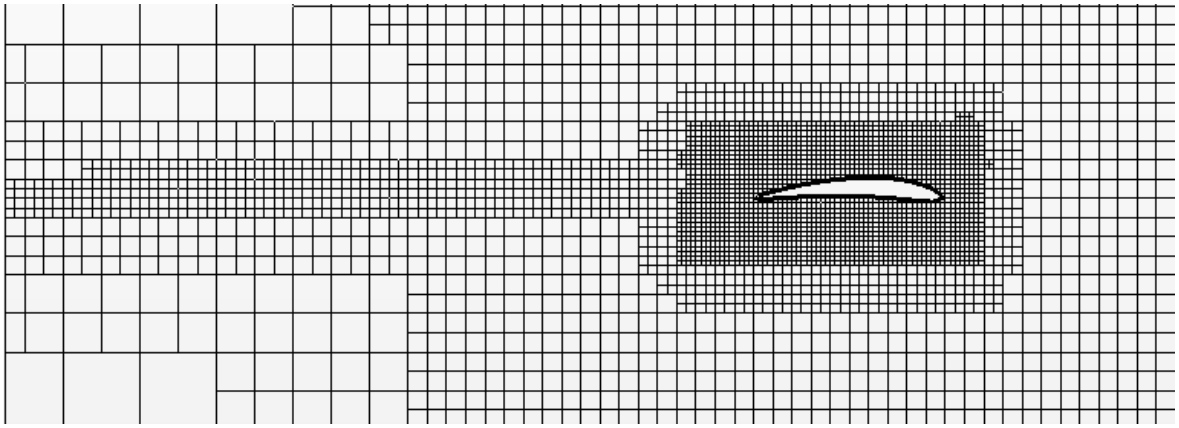

Figure 5.15: WR1 symmetry plane mesh, showing wake refinement

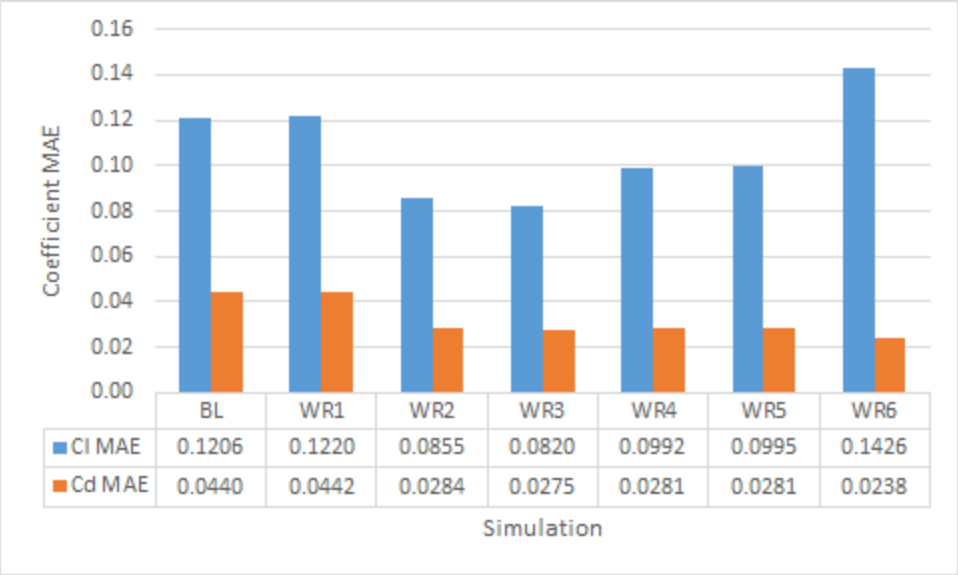

Figure 5.16: MAE for lift and drag coefficients in simulations WR1-WR6

WR2 removed both of the volumetric controls and specific surface refinement for the wing element. It used a wake refinement similar to WR1, but made it longer and used smaller cells. These changes greatly reduced error in both lift and drag coefficients, and seemed to stop the issue of early flow separation. The comparison to wind tunnel results shown in Figure 5.17 does not show an early stall in the CFD results. However, it also does not appear to stall at when the wind tunnel results do, and lift is too high, especially at high angles of attack. The drag results were again consistently too high, but less so than the baseline and other simulations.

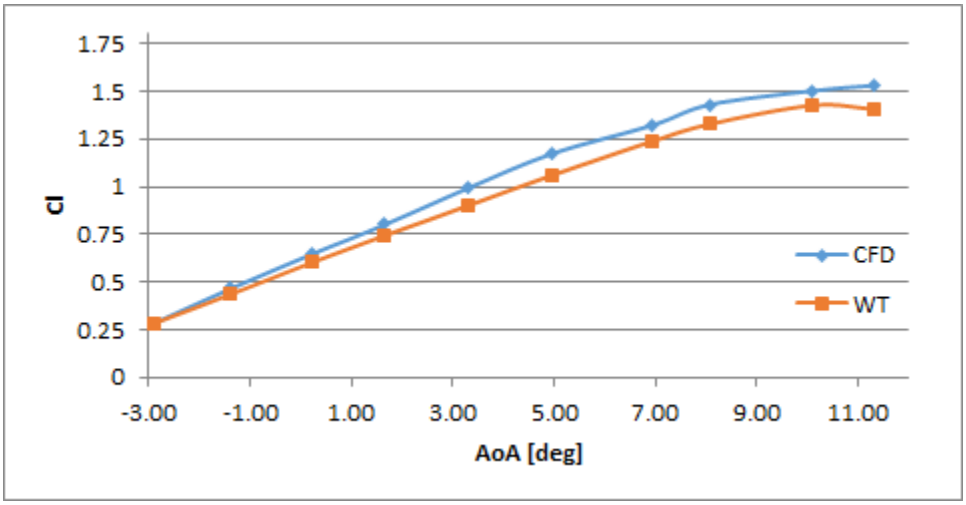

Figure 5.17: Lift coefficient at all angles of attack for WR2, compared to wind tunnel results

WR3 was developed by observing the velocity on the symmetry plane, as shown in Figure 5.18. Regions where black lines are near together indicate high gradients. WR3 added two more wake refinement groups to refine the mesh in the areas with high gradients: a new group was added above the wing, and the refinement region behind the wing was split into two groups to refine it

more near the wing, and less farther away. The resulting mesh is shown in Figure 5.19. This made mild improvements to both lift and drag accuracy compared to WR2, resulting in the most accurate mesh up to this point.

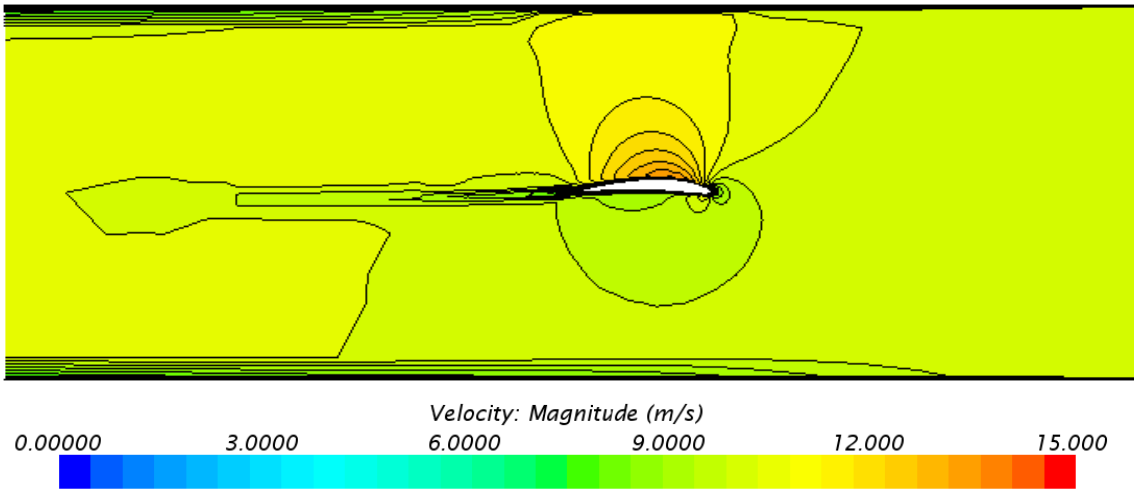

Figure 5.18: Velocity profile on the symmetry plane from BL

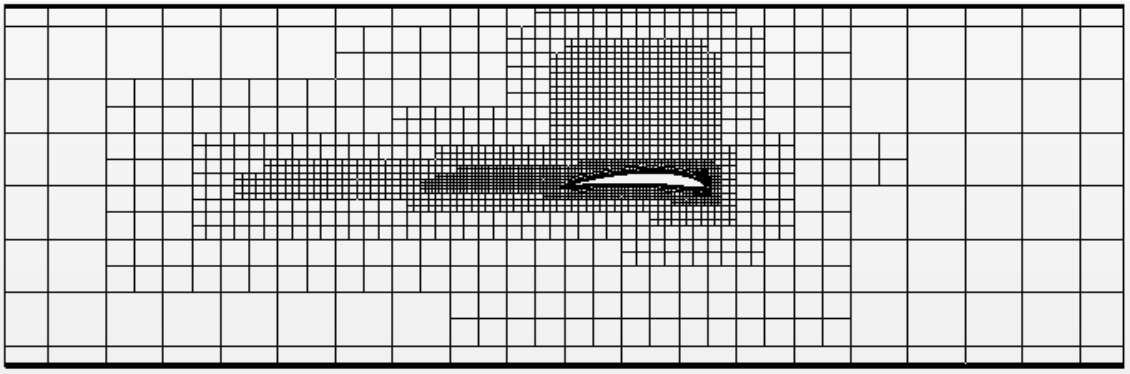

Figure 5.19: WR3 mesh, on the symmetry plane

WR4 started with the WR3 mesh and added and an additional wake refinement group below the wing, labeled "lower wake refinement." It also changed the default growth rate from medium to slow. This lowers the rate that cell size increases moving away from highly refined regions, to create a more gradual transition from small cell size to large cell size. This did not end up being a good result: it both increased cell count and reduced accuracy.

WR5 again started with the WR3 mesh and changed the default growth rate from medium to slow, but did not add any more wake refinement, unlike WR4. The results were almost identical to WR4.

WR6 also started with the WR3 mesh and then changed the prism layer settings to match PL2, the best performing PL simulation. This increased drag accuracy, but greatly reduced lift accuracy. This large reduction in accuracy was unexpected. It suggests that interactions between the prism

layer and the nearby cells are very important in determining accuracy and one particular prism layer setting may not be universally the best.

5.1.4 Physics Models

Physics model (PH) simulations tried out two different turbulence models: k-epsilon and k-omega. They altered boundary condition parameters such as turbulence intensity and turbulent viscosity ratio to fine-tune the models. All physics model simulations used the mesh from WR3, which was the best prior result. PH1-PH8 switched the turbulence model from k-epsilon to k-omega and altered several parameters in attempt to improve the results. These changes are detailed below in Table 5.12.

Table 5.12: Physics model (PH) 1-8 single element simulation parameters

Simulation	Parameter	Value
WR3	Physics model	Realizable k-epsilon two-layer
	Turbulence intensity (initial)	0.01
	Turbulent velocity scale (initial)	1 m/s
	Turbulent viscosity ratio (initial)	10
	Turbulence intensity (inlet)	0.01
	Turbulent viscosity ratio (inlet)	10
	Turbulence intensity (outlet)	0.01
	Turbulent viscosity ratio (outlet)	10
PH1	Physics model	SST (menter) k-omega
PH2	Physics model	SST (menter) k-omega
	Turbulent velocity scale (initial)	1 m/s
PH3	Physics model	SST (menter) k-omega
	Turbulent velocity scale (initial)	22.1564 mph (9.90 m/s)
	Turbulence intensity (initial)	0.05
	Turbulence intensity (inlet)	0.05
	Turbulence intensity (outlet)	0.05
PH4	Wake refinement VC cell size	10 mm
	Wake refinement VC corners	[-1.503, 0.0, 0.302] [-1.093, 0.531, 0.465] [m]
	Others settings same as PH3	
PH5	Turbulent viscosity ratio (initial)	5

	Turbulent viscosity ratio (inlet)	5
	Turbulent viscosity ratio (outlet)	5
	Others settings same as PH3	
PH6	Turbulent viscosity ratio (initial)	1
	Turbulent viscosity ratio (inlet)	1
	Turbulent viscosity ratio (outlet)	1
	Others settings same as PH3	
PH7	Turbulent viscosity ratio (initial)	0.2
	Turbulent viscosity ratio (inlet)	0.2
	Turbulent viscosity ratio (outlet)	0.2
	Others settings same as PH3	
PH8	Turbulent viscosity ratio (initial)	0.1
	Turbulent viscosity ratio (inlet)	0.1
	Turbulent viscosity ratio (outlet)	0.1
	Others settings same as PH3	

PH1 changed the physics model to k-omega, but made no other changes. This marginally decreased error in lift coefficient, and increased it for drag coefficient. It also added the problem that the solution does not converge very well at high angles of attack with significant separation. Instead of converging to a single value, the solution converged to a repeating iterative cycle. To select a final value for a given variable of interest, the last iterations which are part of a cyclic loop were averaged. 500-1000 iterations were typically used. This problem was persistent across almost all simulations using the k-omega turbulence model and led to higher differences in mass flow rate in and out of the wind tunnel. PH2 made the next incremental change by altering the initial condition “turbulent velocity scale” to accurately reflect the free stream velocity in the wind tunnel. PH3 then changed the turbulent intensity initial and boundary conditions from 0.01 to 0.05. These values were based on recommendations from Saxena. Saxena recommends values of 0.01 to 0.1 for internal flows and as low as 0.0005 for external flows [17]. It was estimated that turbulence intensity would be fairly high on the inside of a wind tunnel, but a wide range of values was experimented with later. PH4 attempted to improve the convergence by adding refinement to areas with high variable gradients: in this case, by adding a volumetric control to further refine the wake. The size of this volumetric control is shown in Figure 5.20, compared to the mesh from WR3 and other PH simulations.

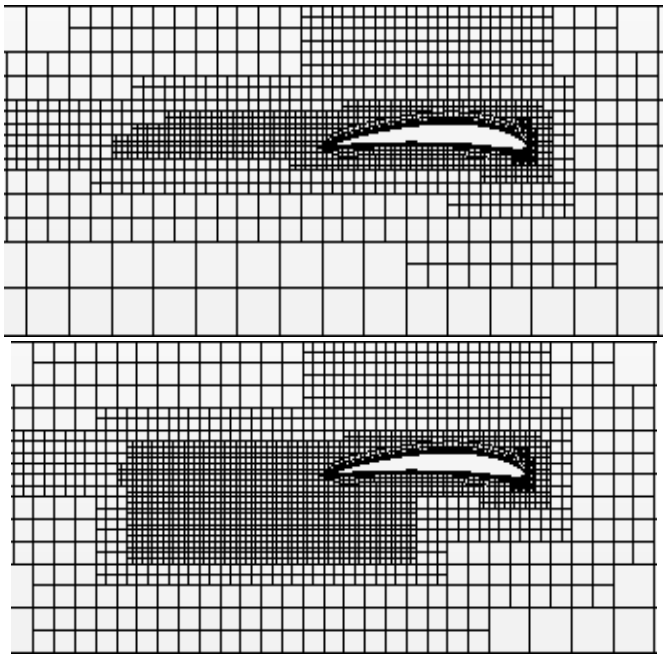

Figure 5.20: WR3 symmetry plane mesh (top), compared to additional wake refinement in PH4 mesh (bottom). All other PH simulations used the WR3 mesh.

This wake refinement change did not improve convergence or accuracy, so it was not used in later simulations. PH5-PH8 used PH3 as a baseline, and altered turbulent viscosity ratio at the initial and boundary conditions in a range from 5 to 0.1, again based on a range recommended by Saxena [17]. The results of these tests are shown below in Figure 5.21.

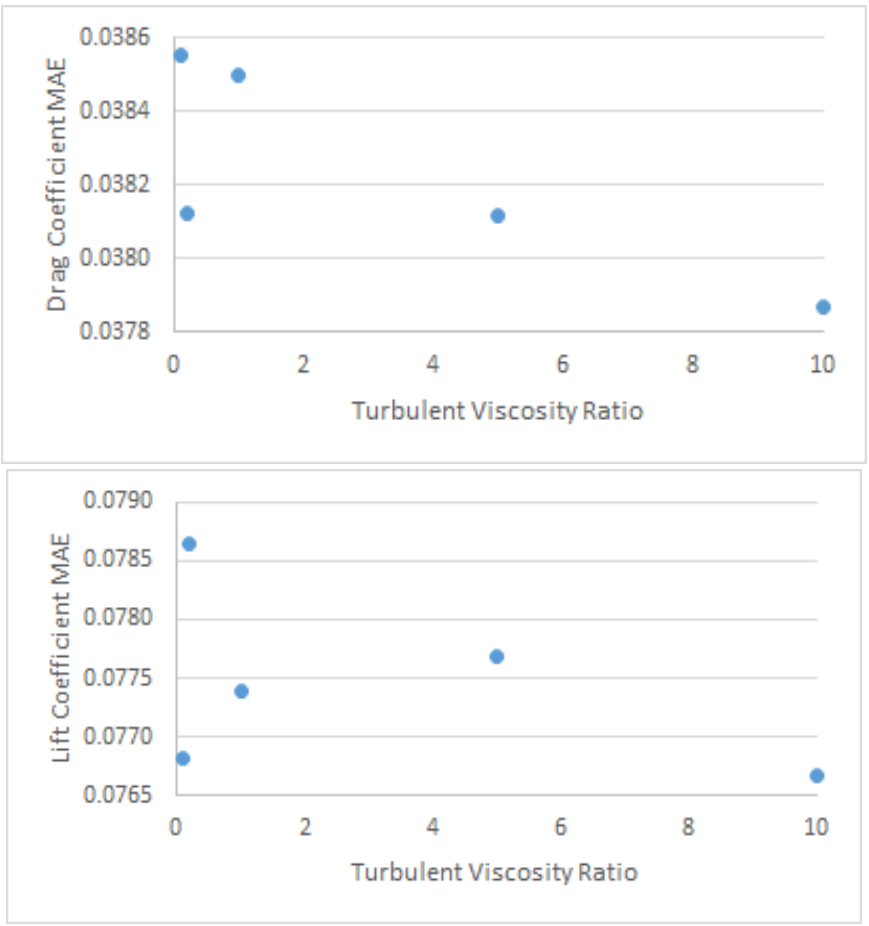

Figure 5.21: Lift (top) and drag (bottom) coefficient MAE for PH5-PH8, compared to PH3.

None of the changes in PH5-PH8 improved over the baseline result from PH3, and there was no clear trend between accuracy and turbulent viscosity ratio. Because of these disappointing results and the difficulty in intuitively selecting a turbulent viscosity ratio, it was decided to use an alternate method to specify turbulence. Instead of turbulent viscosity ratio, turbulence length scale was used along with turbulence intensity. Saxena recommends a turbulence length scale equal to 0.07L, where L is a characteristic length. This was used as an initial guess. The two turbulence parameters were varied in simulations PH10-PH23 to find sensitivity to each. The parameters for each simulation are listed in Table 5.13. The results are plotted below in Figure 5.22 for turbulence length scale and Figure 5.23 for turbulence intensity.

Table 5.13: Physics model (PH) 10-23 single element simulation parameters. For each turbulence parameter, the initial, inlet, and outlet conditions are the same. All other parameters are the same as PH8.

Simulation	Parameter	Value
PH10	Turbulence length scale	0.028 m
	Turbulence intensity	0.05
PH11	Turbulence length scale	0.014 m

	Turbulence intensity	0.05
PH12	Turbulence length scale	0.042 m
	Turbulence intensity	0.05
PH13	Turbulence length scale	0.007 m
	Turbulence intensity	0.05
PH14	Turbulence length scale	0.100 m
	Turbulence intensity	0.05
PH15	Turbulence length scale	0.200 m
	Turbulence intensity	0.05
PH16	Turbulence length scale	0.300 m
	Turbulence intensity	0.05
PH17	Turbulence length scale	0.400 m
	Turbulence intensity	0.05
PH18	Turbulence length scale	0.500 m
	Turbulence intensity	0.05
PH19	Turbulence length scale	0.500 m
	Turbulence intensity	0.1
PH20	Turbulence length scale	0.500 m
	Turbulence intensity	0.01
PH21	Turbulence length scale	0.500 m
	Turbulence intensity	0.005
PH22	Turbulence length scale	0.500 m
	Turbulence intensity	0.001
PH23	Turbulence length scale	0.500 m
	Turbulence intensity	0.0005

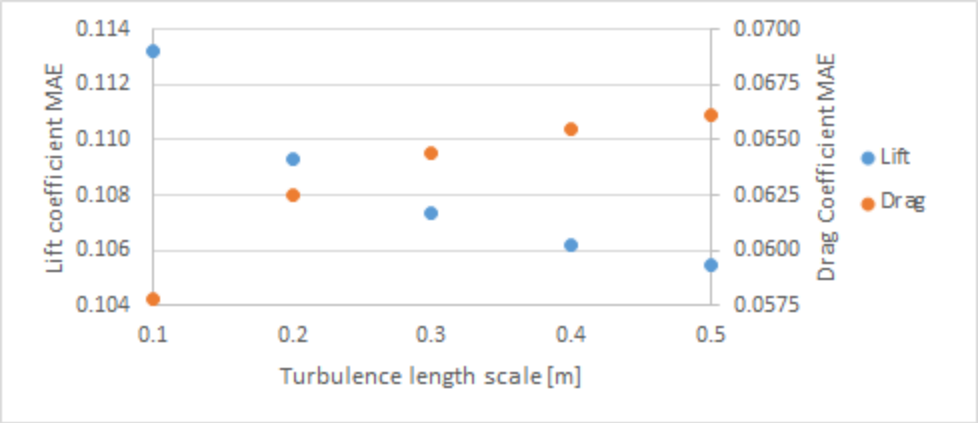

Figure 5.22: Lift and drag coefficient error for varying turbulence length scale with constant turbulence intensity

The sensitivity to turbulent length scale was inconclusive. Error in lift consistently decreased as length scale was increased, but error in drag consistently increased as length scale was increased.

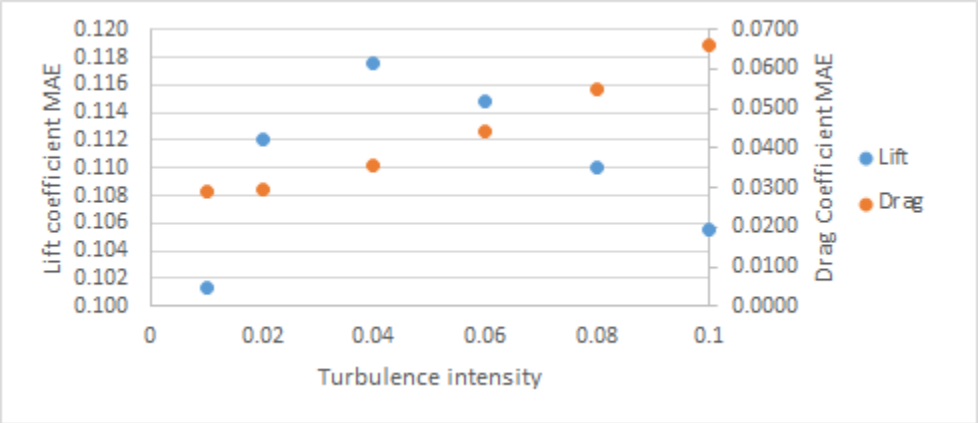

Figure 5.23: Lift and drag coefficient error for varying turbulence intensity with constant turbulence length scale

Error was lowest for both lift and drag when turbulence intensity was lowest, at 0.01. Lift had a local high error with turbulence intensity equal to 0.04, but drag consistently increased as turbulence intensity increased. Because the best performing point is at the limit of the range tested, it is likely that better performing values could exist outside of the tested range. However, these values could be very different for the single element wind tunnel and the GFR car on-track. Because the ultimate goal is to make the model accurate for the GFR car, it was decided there was no benefit to further tuning these parameters in the single element wind tunnel model. These simulations established that these parameters can have a significant impact on the accuracy of the simulation, but the best values for the GFR car will have to be found with other methods.
The remaining PH simulations, PH24-PH33, performed a similar sensitivity study using the k-epsilon turbulence model. Again, turbulence length scale was varied from 0.1 to 0.5 and turbulence intensity was varied from 0.01 to 0.1. The parameters for each simulation are listed below in Table 5.14.

Table 5.14: Physics model (PH) 24-33 single element simulation parameters. For each turbulence parameter, the initial, inlet, and outlet conditions are the same. K-epsilon physics model is used for all simulations; all other parameters are the same as PH8

Simulation	Parameter	Value
PH24	Turbulence length scale	0.500 m
	Turbulence intensity	0.1
PH25	Turbulence length scale	0.400 m
	Turbulence intensity	0.1
PH26	Turbulence length scale	0.300 m
	Turbulence intensity	0.1
PH27	Turbulence length scale	0.200 m
	Turbulence intensity	0.1
PH28	Turbulence length scale	0.100 m
	Turbulence intensity	0.1
PH29	Turbulence length scale	0.500 m
	Turbulence intensity	0.08
PH30	Turbulence length scale	0.500 m
	Turbulence intensity	0.06
PH31	Turbulence length scale	0.500 m
	Turbulence intensity	0.04
PH32	Turbulence length scale	0.500 m
	Turbulence intensity	0.02
PH33	Turbulence length scale	0.500 m
	Turbulence intensity	0.01

5.1.5 Other Tests

A polyhedral mesh was used in simulation M1. Compared to baseline (BL) it increased error in both lift and drag, and appeared to worsen the problem of flow separation occurring at too low of an angle of attack in the simulation. This effect is shown by the early stall visible in Figure 5.24. Because of these initially poor results, polyhedral meshes were not pursued further. It is possible that, with further refinement, error could be reduced. This could be the subject of future testing.

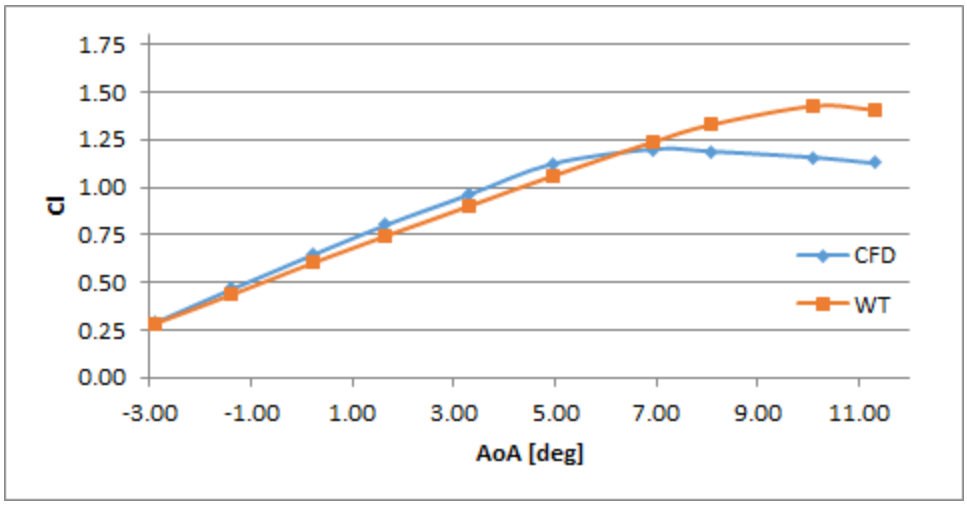

Figure 5.24: Polyhedral mesh (M1) CFD lift coefficient vs angle of attack (AoA), compared to wind tunnel (WT) results.

5.1.6 Best Results

PL17 (based on the physics from PH19) was ultimately found to have the most accurate lift coefficient. Its lift coefficient is plotted vs. angle of attack and compared to baseline CFD and wind tunnel results in Figure 5.25 below. It was very close to the wind tunnel results for all angles except for the 3º-7º range, where it was slightly too high.

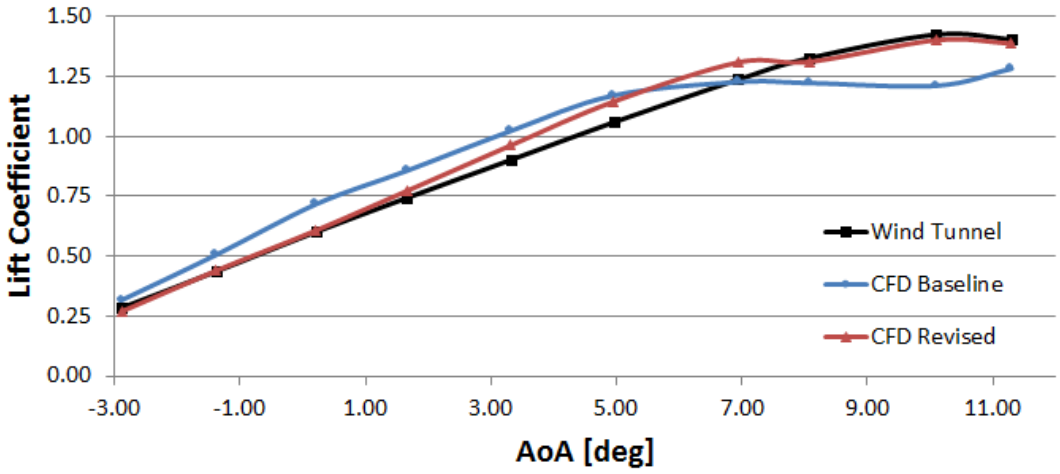

Figure 5.25: Lift coefficient vs. angle attack for baseline CFD, best CFD, and wind tunnel

WR6 had the most accurate drag coefficient, but it was still very inaccurate. The CFD drag coefficient was approximately twice as large as the wind tunnel results at all angles of attack.

5.2 Half-Car Model

The half-car model simulation plan was mostly changed. Yaw, pitch, reverse, and circulation control studies were not completed due to time constraints and other people working on the same topics. The half-car simulation plan was also changed to build a new mesh model, mostly starting from scratch, rather than making incremental revisions to the previous model.

5.2.0 Baseline

The 2015 half-car baseline uses the same mesh and physics parameters as the single element baseline discussed in Section 5.1.0. It contains one half of the car, split in the x-z plane at the centerline. A symmetry plane boundary is used to represent the other half of the car. Volumetric controls are used to refine the mesh around the entire car, and further refine it in the front wing, side wing/undertray, and rear wing areas. Free stream velocity is set to 65 km/h, the average speed at competition. A symmetry plane velocity profile with contours is shown in Figure 5.26 below.

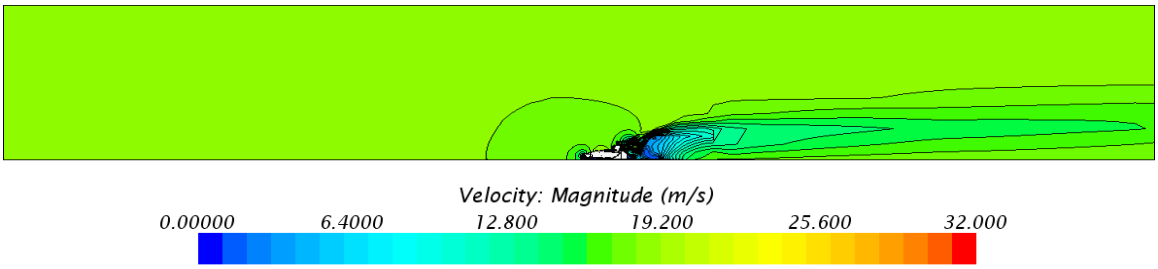

Figure 5.26: Half-car baseline symmetry plane velocity profile

5.2.1 Mesh

The half-car mesh was built systematically using the single-element wing simulation results as guidelines. The overall goal was to accurately represent the surface, refine the mesh most where it is needed, and create a prism layer that accurately captures the boundary layer. The GFR13 car is used because it has physical testing data is available for both downforce and drag.

Volumetric controls are used to refine the mesh, except for at surfaces. While the principles behind wake refinement are useful and valid, it was decided not to use the wake refinement tool. It does not work well with a complexly shaped car and wake, and the same benefits can be achieved with volumetric controls. Volumetric controls were located to provide the most refinement to regions with the largest velocity gradients. These high gradient regions can be seen where contours are close together in Figure 5.26. It was also noted that the airflow is disrupted in a large wake behind the car, but only in a small region in front of it. The simulation boundaries were therefore moved to include more space behind the car, and less in front of it. This change is supported by CD-adapco's recommended settings. The final locations of the car and volumetric controls are shown below in Figure 5.27. Volumetric controls are defined with six rectangular regions, divided into four levels of refinement.

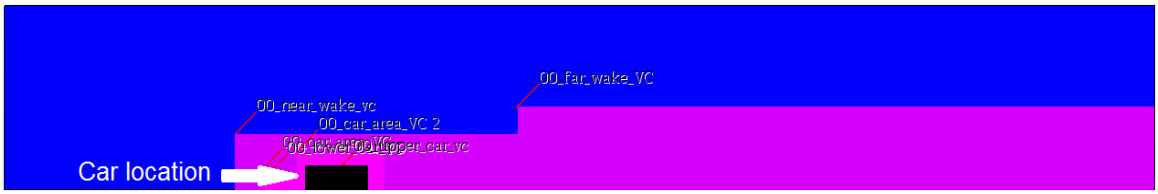

Figure 5.27: Half-car simulation cross section. Volumetric controls are shown in pink.

One major issue that arose while experimenting with volumetric controls is that the mesher will not always make cells exactly to a specified size. The trimmer mesh limits the main region of the mesh (outside of prism layers) to having cells scaled by a factor of two compared to their neighbors. For example, a cell with a size of 1m may only have neighboring cells of size 2m, 1m, or 0.5m. To work with this constraint, an incremental series of refinements is created. The mesh base size is 1m, and refinements exist at 0.5m, 0.25m, 0.125m, and so on. All refinements are defined relative to the base size to allow the entire mesh to be refined easily. The overall layout of cell density in the simulation is shown in Figure 5.28.

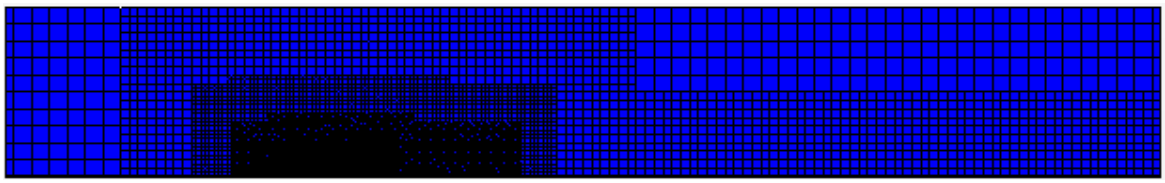

Figure 5.28: Half-car symmetry plane mesh, showing cell density

There are four levels of volume refinement, designated: car detail, car area, near wake, and far wake. "Car detail" covers the areas closest to the car and the wake immediately behind it, as shown in Figure 5.29. "Car area" extends the dimensions of "car detail" slightly in every direction and extend the wake region much further rearward, as shown in Figure 5.30. "Near wake" covers a larger area around the car and extend farther rearward. "Far wake" extends from the back end of "near wake" to the end of the wind tunnel. These regions were chosen based on the velocity gradients from Figure 5.26.

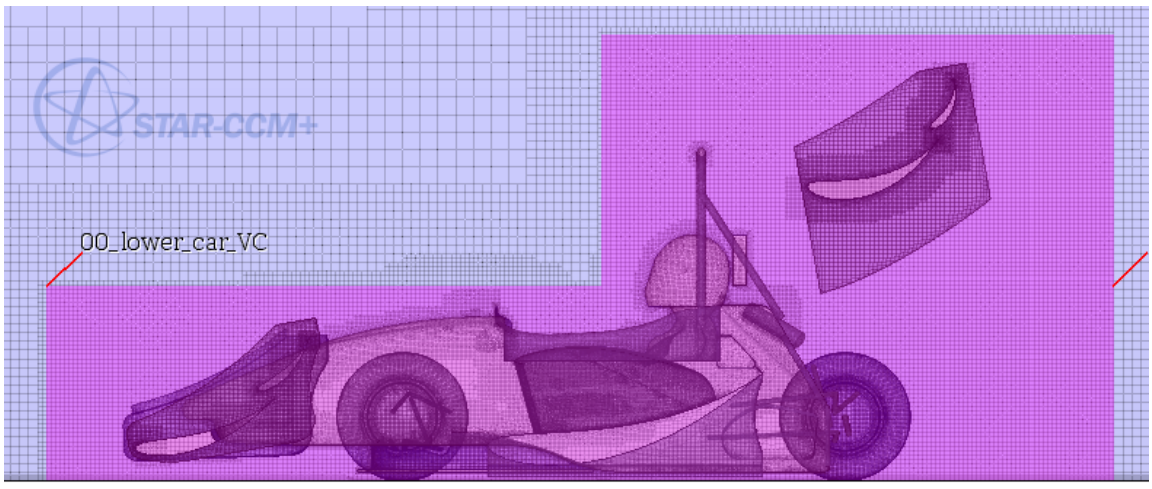

Figure 5.29: "Car detail" volumetric control, with symmetry plane and surface mesh shown.

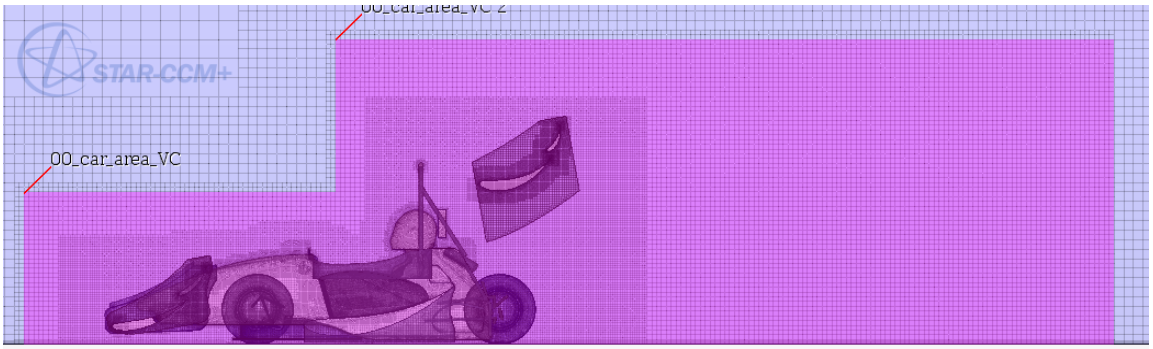

Figure 5.30: “Car area” volumetric control, with symmetry plane and surface mesh shown.

Surface refinement was done per part, not using volumetric controls. Because the vast majority of parts in the simulation are car parts, the global settings were used to define the correct surface size for these parts. The simulation (“wind tunnel”) walls were changed at the part level to have larger surface sizes. Global surface size was set to target 0.015625m (1/64 m) with minimum size 0.0039m (1/256 m). This minimum size allowed reasonable accuracy for small radius curves and the target size was appropriate to create a reasonable number of cells. Larger and smaller surface sizes were experimented with. A smaller minimum surface size (1/512 m) resulted in too many cells (~8 million) and a larger one (1/128 m) resulted in loss of detail on small radius parts, such as wing leading edges and suspension links. Surface size was set to target 1m and minimum 0.25m for the “wind tunnel” walls, but these dimensions are overridden for smaller cells near the car. The final surface in the volume mesh is shown in Figure 5.31.

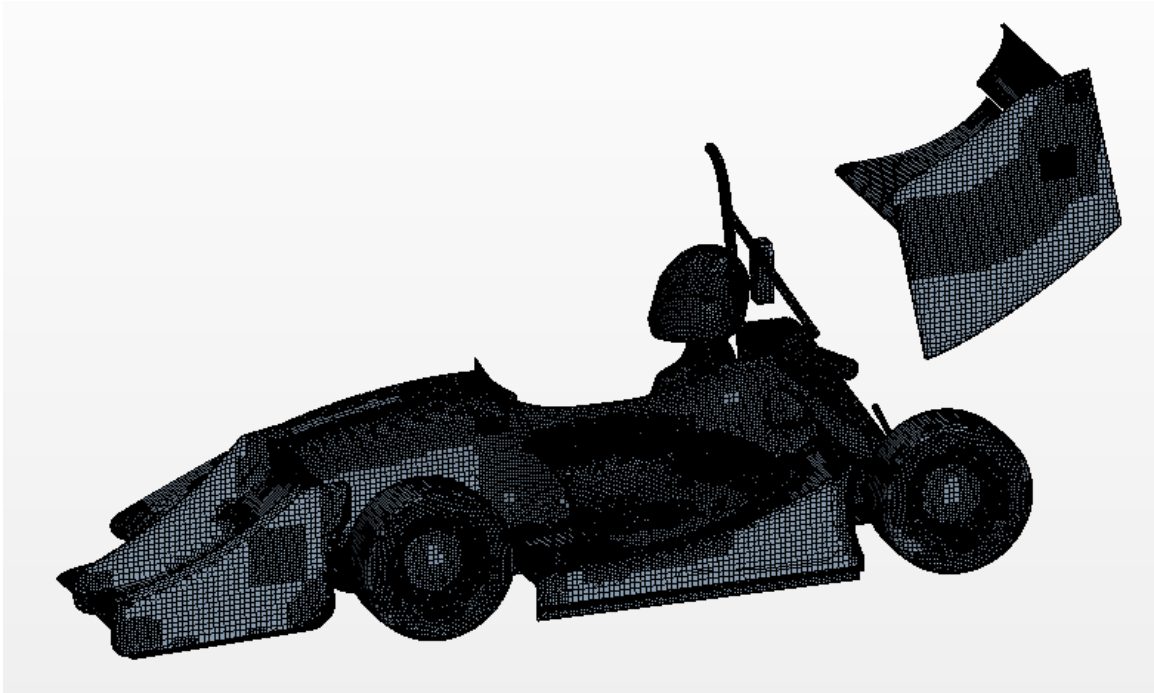

Figure 5.31: Final half-car surface in volume mesh

Prism layers were set globally to have 5 layers and be 20mm thick. This was adapted to keep wall y+ values in the log-law region, but resulted in high values in some regions, as shown in Figure 5.32. It was difficult to put all y+ values near the same level because of varying airspeed, especially on the upper and lower surfaces of wings. Very little sensitivity analysis was done in this area, so this is an area to target for future development.

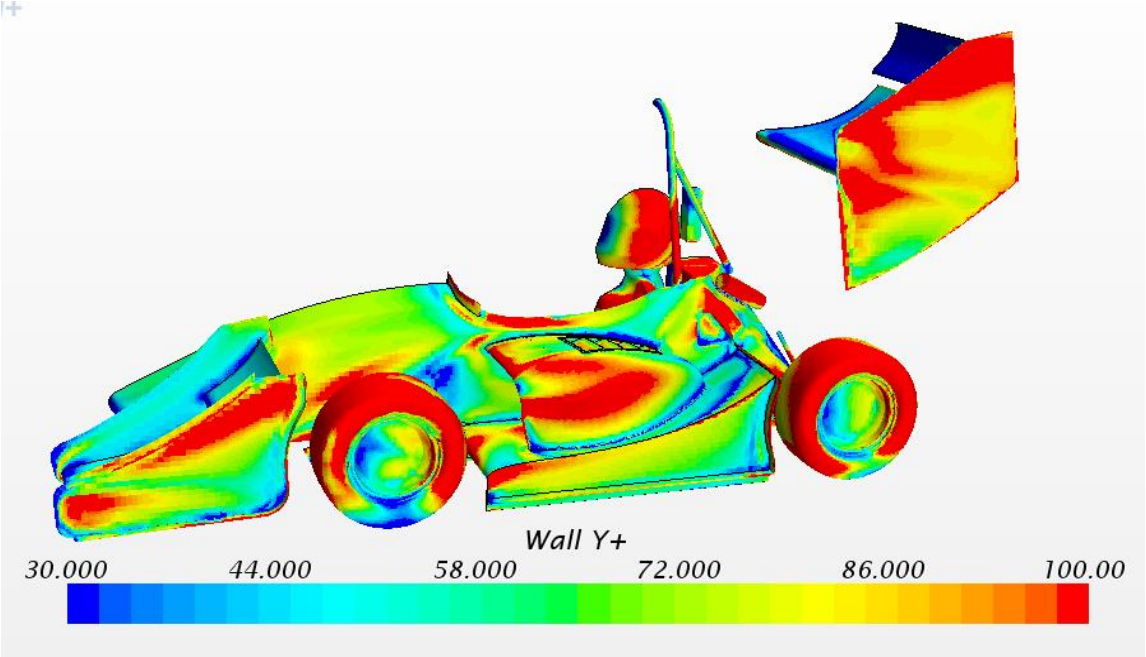

Figure 5.32: Wall y+ on half-car mesh

The resulting mesh has 3.4 million cells.

5.2.2 Physics

The final mesh was initially run with the k-epsilon physics model. It converged in about 1500 iterations, and gave the results of 867 N downforce and 392 N drag. It was then run with the k-omega physics model. This created serious convergence issues, illustrated the downforce/drag per iteration plot shown below in Figure 5.33. Residuals remained high (>0.1) and were not improved by under-relaxing. Further investigation and simulation will be needed before this can be feasibly used for design purposes.

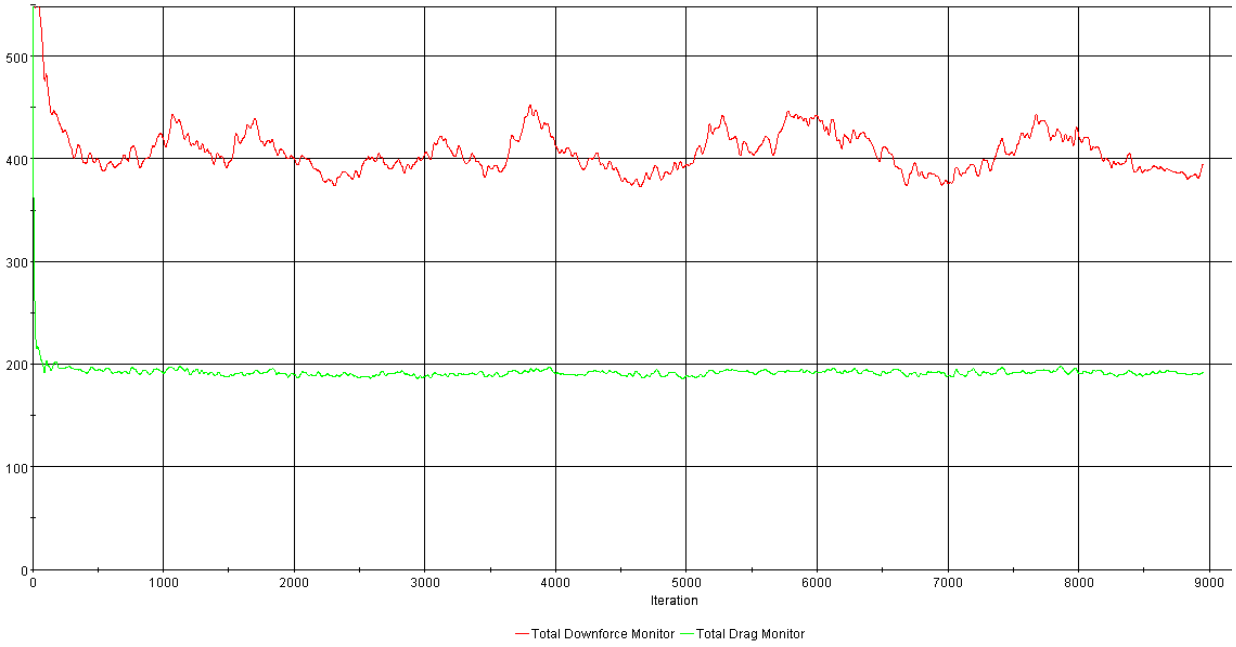

Figure 5.33: Total downforce [N] and Total drag [N] vs iteration number for GFR13car

The final 5000 iterations, covering about two major cycles, were averaged to find total downforce and drag values of 808 N and 383 N, respectively. This is 7% lower downforce and 2% lower drag than the k-epsilon results. This may mean that the k-omega physics model results in lower downforce and drag values, or it may be meaningless due to the high error indicated by high residuals.

5.2.3 Comparison to Physical Data

The 2013 physical testing results found 1066 N downforce and 397 N drag at 65 km/h [18]. This is 23% higher downforce and 1.2% higher drag than the k-epsilon physics model results. The drag results are satisfactory, but the downforce difference is much larger than expected. One possible reason for this is that the physical testing downforce results are based on air speed from the Pitot tube. On the GFR13c car, the Pitot tube was located at the top of the roll hoop. At this location, the CFD results show an air velocity of 17.04 m/s, which is lower than the free stream 18.05 m/s. Given this discrepancy, the Pitot tube will report a lower speed than the car is actually traveling, and the calculated downforce will be too high. Taking this into account, a better estimate of actual downforce is 970 N. This is still 11.9% higher than CFD results. Overall, not very much sensitivity analysis was done with the half-car model due to time constraints. Further simulation should be done in these areas to bring the downforce results closer to physical testing data, and further physical testing should be done to verify the limited results we have.

5.3 Other Notes

5.3.1 Assessing Convergence

It can sometimes be difficult to determine when a simulation has iterated to convergence with sufficient accuracy. A solution that is not converged can produce inaccurate or incorrect results. It is therefore important to have a well-defined and consistent method to evaluate iteration convergence. Three related measures are listed below:

1. Continuity: Because GFR uses steady state (and incompressible) conditions, mass flow rates into and out of the domain should be equal in a converged solution. This can be measured using mass flow rate reports at the inlet and outlet boundaries. A large discrepancy indicates that the simulation is not converged. It is important to note that a small error in this parameter alone is not sufficient evidence to determine a solution is converged [19].
2. Residuals: Residuals are normalized measures of the rate of change of dependent variables in the governing equations (continuity, Navier-Stokes, turbulence models, etc.) used by the simulation. For GFR simulations, these include x-, y-, and, z-momentum; continuity; and turbulence model variables such as turbulent kinetic energy (k or Tke), turbulent dissipation rate (ε or Tdr), and specific dissipation rate (ω or Sdr). These are automatically recorded and reported in a plot by Star-CCM+. As a rule of thumb, a simulation cannot be considered converged if any residuals are greater than 10^{-3}, and smaller values are desired [19]. GFR routinely reaches convergence with residuals around 10^{-4} or 10^{-5}.
3. Parameters of interest: For GFR, these parameters are typically downforce and drag for the entire car or a specific part, such as the front wing. These parameters are measured using force reports in Star-CCM+. Because an accurate result is desired for these parts, the solution should not be considered converged if they are changing significantly with new iterations. This can be measured using a fairly simple definition, such as requiring that downforce change by less than 1N in the last 100 iterations. It could also be measured using a more professional definition, such as Ferziger's equation for iteration error [20].

In an iteratively converged solution, all three of these measures should show small error. Based on experience running simulations for GFR, the error in parameter of interest is typically the last condition to be met. For this reason, I recommend that downforce and drag numbers should be monitored and when the rate of change is sufficiently small, the simulation can be stopped. Continuity and residuals should be used to verify iteration convergence. Of course, it is possible to monitor all three measures simultaneously, but this is additional work for the user and ultimately unnecessary as long as continuity and residuals are checked at the end.

6. Testing

6.1 Tests Complete to Date

The simulations are "tested" through comparison to wind tunnel data and on-track data for the single element and GFR car, respectively. Methods for each category are described below.

6.1.1 Single Element Wind Tunnel Model Validation

The single element model is validated through comparison to wind tunnel data from Selig et al. [16]. CFD simulations were run at the same angles of attack and Reynolds numbers to match the experiments. Quantitative comparison it done by calculating a mean approximate error (MAE) across all angles of attack, assuming the wind tunnel data is the "correct" value. Qualitative comparisons can also describe the nature of the error, such as early stall. The CFD accuracy can also be validated by calculating parameters such as iteration error, grid convergence error, and mass flow rate error. Discussion of these validation methods is included in Section 5, above.

6.1.2 Half Car Model Validation

The half-car model is validated by comparison to on-track tests with GFR cars. The cars are driven in straight line "coast-down" runs, which can be used to find values for downforce and drag at different speeds [21]. Strain gages and linear potentiometers can be used to measure suspension strain and travel, which can be used to determine downforce. A Pitot tube measures air speed, and wheel speed sensors can measure wheel speed. Drag can be determined from the deceleration rate. Rolling friction and other losses must either be estimated or neglected for this analysis [22].

To date, these tests have not been completed on the GFR15 car, and data from GFR14 has not been resolved into downforce and drag numbers.

6.2 Tests to Complete

Coast down tests should be completed with the GFR15 car. Yaw CFD could be better developed as well, and validated through comparison to constant radius turn tests. The CFD model robustness can be further validated by changing parameters such as wing angle of attack and seeing if CFD results remain valid in different conditions. CFD simulations should be run at different vehicle speeds for the same reason.

After putting a lot of time into developing CFD, GFR has a model that is probably fairly good, but cannot be further validated without more measured data. I think GFR should focus more on developing and performing on-track or wind tunnel tests to validate the CFD model, or try out parts such as gurney flaps and vortex generators that we are not confident we can model accurately in CFD. These are areas that GFR does not have much data from, and I think these are the places where we will find the most benefit per time spent.

In CFD, we should explore mesh generation more, and look into different software to generate meshes. Dedicated meshing software is considered to create better meshes than Star-CCM+, and these can be imported into Star-CCM+ to run. We should also try to find the source of poor convergence when using the k-omega model, and figure out how to resolve it.

7. Conclusion

As mentioned above in the testing section, I think it would be more beneficial in the future to have a more "testing and validation" oriented senior project than another CFD project. I think it would still be good for the senior completing this project to have some familiarity with CFD for comparison and validation. I found the CFD class (ME 567) to be very helpful in understanding the nuances of CFD, and I would highly encourage any senior doing CFD development to take it (it is not necessary if the senior is just running CFD in already developed models). I think this project should be done in the winter-spring section to allow for data collection during spring testing and to allow the senior to take ME 567 during winter term, if further CFD development is being done.

For senior projects in general, I have noticed that they tend to go better if the expectations and deliverables are very clear. This is usually done pretty well with projects that involve designing and manufacturing a part, but other projects have been less focused. Having a clear deliverable can both make it easier for the senior to figure out what they need to do, and motivate them to do it. I think in the future, we should especially try to set clearer goal for the aero manufacturing project--designing and manufacturing molds and fixtures, and making sure they are done early. From a manufacturing standpoint this year, I think we did not focus enough on fixturing and bonding until the last minute. Molds arriving late was another large issue, but one that was largely out of our hands. It would probably still be a good idea to plan very far ahead with molds too large to be machined in house.

8. Works Cited

[1] Takaro, T. (2014). "Equating design parameters to points." Global Formula Racing Private Wiki.

[2] SAE International (2014). "2015 Formula SAE Rules, Revision 9/17/2014." SAE International.

[3] Cox, B. (2013). "2013 CFD Report OSU." Global Formula Racing Private Home.

[4] Birkenmaier, J. (2011). "2011 CFD Improvement." Global Formula Racing Private Home.

[5] Duschek, D. (2012). "2012 GFR Slot Gap Testing." Global Formula Racing Private Home.

[6] Peterson, C. (2014). "Three Element Rear Wing Slot Gap CFD Analysis and Wind Tunnel Validation." Oregon State University Undergraduate Thesis.

[7] CD-adapco (2013). "Workshop: External Aerodynamics of a Simple Race Car Geometry." *CD-adapco*.

[8] Global Formula Racing (2015). "Aero run/ran." Google spreadsheet.

[9] CD-adapco (2013). "Best Practices for Vehicle External Aerodynamics."

[10] Nunn, R.H. (1989). *Intermediate Fluid Mechanics*. New York: Hemisphere Publishing Corporation

[11] CD-adapco (2014). "STAR-CCM+ 9.04.011 Documentation File." CD-adapco.

[12] Salim, S.M., and Cheah, S.C. (2009). "Wall y+ Strategy for Dealing with Wall-bounded Turbulent Flows." Hong Kong: International MultiConference of Engineers and Computer Scientists.

[13] CD-adapco (2014). "Tutorials For STAR-CCM+, FSAE." YouTube Playlist.

[14] Maneia, G. M. (2007) "Aerodynamic study of airfoils and wings for power kites applications" Master's Thesis.

[15] Frei, W. (2013). "Which Turbulence Model Should I Choose for my CFD Application?" COMSOL Online Documentation.

[16] Selig, M.S., Guglielmo, J.J., Broeren, A.P., and Giguère, P. (1995). *Summary of Low-Speed Airfoil Data* (Vol. 1). Virginia Beach, VA: SoarTech Publications.

[17] Saxena, A. (2007). "Guidelines for Specification of Turbulence at Inflow Boundaries." ESI CFD Customer Portal.

[18] Global Formula Racing (2013). "GFR 2013 Coast Down Testing" Global Formula Racing Private Home

[19] Versteeg, H.K., and Malalasekera, W. (2007). *An Introduction to Computational Fluid Dynamics* (2nd Ed.). Harlow, England: Pearson.

[20] Celik, I.B., Ghia, U., Roache, P.J., and Freitas, C.J. (2008). "Procedure for Estimation and Reporting of Uncertainty Due to Discretization in CFD Applications." *Journal of Fluids Engineering* 130(7).

[21] McBeath, S. (2011). *Competition Car Aerodynamics* (2nd Ed.). Sparkford, UK: Haynes Publishing.

[22] Katz, J. (1995). *Race Car Aerodynamics: Designing for Speed*. Cambridge, MA: Bentley Publishers.